공학박사학위논문

비틀림파의 산란 이론과 복수의 비틀림 모드를 활용한 노치 결함의 정량화 기법

Torsional wave scattering theory in a pipe and notch defect characterization using multiple torsional wave modes

2014 년 8 월

서울대학교 대학원

기계항공공학부

권 영 의

ABSTRACT

Torsional wave scattering theory in a pipe and notch defect characterization using multiple torsional wave modes

Kwon, Young Eui

School of Mechanical and Aerospace Engineering

The Graduate School

Seoul National University

This work is concerned with the development of quantitative characterization of a part-circumferential notch defect in a pipe. Although there are some works that dealt with notch size estimation, there still remain issues to be addressed for full characterization. The aim of this study is to develop a notch characterization method for considerably-improved characterization of notch defects in a pipe. For the characterization, we propose to utilize only the first torsional wave mode at a frequency higher than the second cut-off frequency and measures reflections of multiple torsional wave modes (the first, second and third modes). No earlier

method used higher torsional wave modes although there were some attempts to use higher flexural wave modes. The advantage of using torsional wave modes over other modes is that they are axisymmetric; the magnitudes of reflection coefficients, regardless of mode orders, increase linearly with the central angle of a notch defect. Therefore, the ratios between the magnitudes of the reflected wave modes can be directly used for defect characterization. Specifically, the depth and length of a notch defect can be estimated from the reflection coefficient ratios of the second mode to the first mode and third mode to the first mode while the central angle of a notch can be predicted from the fact that the magnitude of the reflection coefficient of the torsional modes always linearly varies with the central angle.

For quantitative characterization of the size of a notch defect, reference data for a notch defect are needed. Unlike previous methods that demand three-dimensional simulations, the developed method requires only axisymmetric results because all torsional wave modes are axisymmetric. Thus, we only need a defect scattering theory only for axisymmetric torsional waves. By using this theory, equi-reflection coefficient ratio contours for second and third torsional wave modes are prepared and used for the defect characterization. To use the constructed contours, one needs to measure experimental signals but before they are used, they are processed by the dispersion compensation method because of dispersion. With the compensation method, dispersions from higher-order torsional wave modes are suppressed and the signals right at the moment of reflection can be traced back. The compensated signals are then used in using the refection coefficient ratio contours. The developed axisymmetric notch scattering theory is checked experimentally. For the

validation, several defect characterization experiments were conducted in a pipe having artificial notch defects.

Keywords: Notch characterization, Axisymmetric notch scattering theory, Size estimation, Multiple torsional wave modes, Reflection coefficient

Student Number: 2008-22867

TABLE OF CONTENTS

LIST OF TABLES

LIST OF FIGURES

CHAPTER 1.

Introduction

1.1 Motivation

Cylindrical structures have been broadly used in many industrial sites such as gas or oil pipe lines. These infrastructures cause enormous social dislocation when they are under serious damage by defect such as corrosion or crack. Thus a method to nondestructively diagnose defective pipeline installed in a system has been required and researched [1-9]. Among various pipe inspection methods [10-16], guided wave technique has been preferred owing to its own merits; rapid and long range inspection [14, 17-19]. A fundamental matter of inspecting is that to generate a guided wave for measuring the reflected waves from the defect. The existence of defect and its axial location can be found via this guided wave based inspection.

Although guided wave based pipe inspection technique has the advantage in examination speed, there is a limit that it is unable to obtain detailed information about the defect such as size and shape. In order to overcome these problems, roughly two kinds of researches have been developed. The first type is imaging technique and the second type is analysis for reflection coefficients of various guided wave modes. Imaging of pipeline structure has a good advantage not only to demonstrate the presence or location of the defect but also to identify the size or

shape of it [20-22]. However experiment and imaging process are time consuming and required complex devices and the number of transducers. Researches for the reflection coefficients of various guided wave modes have been conducted changing notch parameter [23-25]. Although various kinds of researches have been established, there is no research which quantitatively predicts all parameter of notch defect. The fact that the length of notch defect is quantitatively predicable has been reported [23-26]. For the other variables of notch such as depth and circumferential extent, patterns of reflection coefficients for specific guided wave modes have been observed. Besides quantitative size estimation method for a part circumferential notch defect has not been established yet. In this research to strengthen advantages of guided wave based inspection, reflection coefficients based defect characterization method has been investigated.

Previous works concerned with reflection coefficients for a notch defect have analyzed reflection coefficients with respect to the incident wave; longitudinal mode, L(0,2), or the lowest torsional mode, T(0,1) [23-25, 27]. The symbols L, T and F (for later) denote longitudinal, torsional and flexural modes, respectively. And the first and second indexes represent the harmonic number of circumferential variation and a counter variable respectively, by following Silk and Bainton [28]. When an incident L(0,2) or T(0,1) reaches at the part circumferential notch defect, not only reflection of L(0,2) or T(0,1) itself but also reflection of the flexural modes according to mode conversion occur. For the circumferential extent, the facts that reflection coefficient of L(0,2) or T(0,1) shows linear trend to the circumferential extent of a notch. On the other hand amount of the reflected

flexural modes repeatedly increase and decrease as the circumferential extent of notch defect increases, depending on circumferential order *m* have been reported. This phenomenon is caused by differences of circumferential mode shapes. Otherwise the longitudinal and torsional wave have uniform mode shape in the circumferential direction, the flexural modes have non-uniform mode shape which can be represented as trigonometric function of $m\theta$, where *m* denotes circumferential order [29, 30]. For the depth of a notch defect, reflection coefficients of longitudinal and torsional wave modes have monotonically increasing tendency.

But most established researches have dealt with parametric studies about notch defect, not suggested complete method to characterize size of a part circumferential notch. Because each mode (among longitudinal and flexural modes, or torsional and flexural modes) has similar (not the same) mode shape in the thickness direction, reflection coefficients of each mode do not have significant differences with respect to the thickness of the notch defect. From these results, it has been only to demonstrate potential of notch characterization; selection of one (or some) candidate among the references obtained by three-dimensional simulation. However this probability for notch characterization has not been considerably advanced into integrated sizing method for notch depth and circumferential extent. Because there is no clear index between shape of notch defect (depth and circumferential extent) and mode shape of reflected waves (longitudinal and flexural modes, or torsional and flexural modes). Compare with the notch length case that length of a notch defect can be easily estimated through measuring

reflection coefficients for incident waves having different frequencies. Notch length and wavelength have a close relation independently from notch depth and circumferential extent. Moreover, using flexural waves causes another problem, need of three dimensional references. To characterize notch size based on reflection coefficients, pre-calculated references are necessary. By the way, because flexural modes are non-axisymmetric, three-dimensional analysis which needs heavy computing resources and time are necessary.

To overcome the limitations of previous researches and to investigate a new notch defect estimation method, reflection coefficients, of only the torsional wave modes which are axisymmetric, based notch defect characterization method which needs only two-dimensional reference is developed in this study.

1.2 Research Objectives

The main objectives of this research are two folds: one is to estimate size of a part circumferential defect in a simple experiment and the other is to investigate axisymmetric notch defect scattering theory which will be used as a reference. And this research also includes development of subsidiary objective for crack characterization such as experimental system, signal processing technique and size estimation algorithm.

Objective 1: Development of the axisymmetric notch defect scattering theory

As a reference to characterize size of a part circumferential notch defect, the axisymmetric notch defect scattering theory is proposed. Through this theory

reflection coefficient map for a notch defect having various depth and length can be calculated. And through supplemental processing in Fourier domain reflected signal at the moment of reflection for each torsional wave mode can be obtained for a specific input pulse (in this research, Gabor pulse).

Objective 2: Ratio between reflection coefficients

A new concept, ratio between reflection coefficients, is proposed to predict size of notch defect especially depth and length. Because only the torsional wave modes which are axisymmetric are measured, effect of central angle of notch defect can be ignored. Using this, size of the notch defect can be characterized from the two-dimensional (axisymmetric) notch scattering theory.

Objective 3: Signal processing; dispersion compensation

Unlike the lowest torsional wave having non-dispersive property, higher torsional modes are dispersive which cause that signal of reflected higher torsional wave modes spread. Thus signal processing to reduce effect of dispersion property should be employed. To this end, dispersion compensation method [31] is applied which can suppress dispersion phenomena and trace back the signals right at the moment of reflection. By utilizing this, experimental results can be compared with reference signals.

Objective 4: Development of notch defect size estimation algorithm

By putting together previous objectives, size estimation algorithm for a part circumferential notch defect is investigated. Size of the notch defect can be quantitatively identified with one single experiment. This characterization algorithm is constructed with ease as can evaluate directly.

Objective 5: Experimental validation and real notch defect characterization

The proposed theory needs to be validated experimentally. And through the proposed notch characterization algorithm, artificial notch defects are predicted quantitatively.

1.3 Outline of Thesis

In Chapter 2, the theoretical backgrounds of the stepped rod scattering theory are reviewed. From this, stepped pipe scattering theory is developed. Definition of the power normalized mode shape function for the torsoinal wave modes is presented and modal analyses will be carried out to calculate reflection coefficients of each reflected or transmitted wave mode. The proposed stepped pipe scattering theory is validated numerically. Signal processing technique, dispersion compensation, is applied to numerical result to compare with the results of scattering theory.

In Chapter 3, stepped pipe scattering theory presented in Chapter 2 is expended to axisymmetric notch scattering problem. To this end multiple scattering of stepped pipe case is considered. Notch scattering theory is validated by two-dimensional finite element simulation.

In Chapter 4, effect of the central angle of notch defect is analyzed first. To this end, three dimensional numerical simulations are carried out. Through the results, a new-concept ratio between reflection coefficients is introduced. Using these ratios, which are independent to the central angle of notch defect, possibility of notch

defect characterization is presented.

In Chapter 5, size estimation method for a notch having known length cases is presented. This method is validated experimentally and usefulness of proposed method is verified.

In Chapter 6, crack characterization method presented in chapter 5 is expended to the full characterization. The algorithm for notch defect estimation is proposed which is validated experimentally. Defect characterization experiments are conducted in a pipe having artificial notch defects. At the end of this chapter, limitations and supplementations for the proposed method are presented.

In Chapter 7, the conclusion remarks for this research will be presented.

CHAPTER 2.

Stepped pipe scattering theory

In this chapter, scattering phenomena for a stepped pipe will be carried out. To this end previous research about a stepped rod problem [32] will be reviewed in section 2.1. This theory will be extended to a stepped pipe problem in section 2.2 which is purpose of this chapter. In section 2.3, results of stepped pipe scattering theory compared with finite element simulation will be represented.

2.1 Back ground theory in stepped rod scattering problem

In this section, stepped rod scattering theory [32] that has been previously reported is reviewed with some change of several notations to reinforce contents of a stepped pipe scattering theory in the next section.

2.1.1 Definition of the power normalized mode shape function

The displacement of the torsional waves, in the cylindrical coordinate system shown in figure 2.1 for a uniform homogeneous rod having radius *R*, can be written

$$u\left(\vec{r},t\right)=u_{\theta}\left(r\right)\exp\, j(\xi \mathrm{z}\text{-}\omega \mathrm{t}) \tag{2.1}$$

u_{θ}, mode shape function, can be given by suppressing exponential part

$$u_{\theta}=\begin{cases} A_0K_0^2r, & s=0, \\ A_sk_rJ_1(k_rr), & s>0, \end{cases} \tag{2.2}$$

where *s* denotes number of mode, $\xi^2=K_0^2-k_r^2$, $K_0=\omega/V_t$, $k_r=Z_s/R$, and Z_s is the *s*-th zero of $J_2(Z)$. V_t and ω are shear wave velocity and angular frequency, respectively.

Total power of a given mode can be expressed as

$$P=\int_0^{2\pi}\int_0^R p\,r\,dr\,d\theta\,, \tag{2.3}$$

where *p* denotes Poynting vector in the z direction represented as

$$p=-\frac{1}{2}\left(v^*\cdot T\right)_z. \tag{2.4}$$

By substituting equation (2.4) to (2.3) and using definition of velocity and stress components which are well organized to match the current conditions $v=\partial u/\partial \mathrm{t}$, $T_4=T_{\theta z}=\mu\left(\partial u/\partial z\right)$, we can write total power *P* for any given mode *s*

$$P=\pi\omega\mu\xi\int_0^R u_{\theta,s}u_{\theta,s}rdr \tag{2.5}$$

where μ is shear modulus having $\mu=\rho V_t^2$. Magnitude of mode shape function, A_0 and A_s, in equation (2.2) can be decided to define total power *P* for all *s* values

$$P = \begin{cases} 1, & \text{for propagating modes,} \\ -j, & \text{for cut-off modes.} \end{cases} \tag{2.6}$$

This condition was chosen to satisfy that wave number ξ should be real positive for propagating modes or negative imaginary for cut-off modes. Finally power normalized mode shape function can be obtained by adjusting this condition with respect to equation (2.2) (see reference [32] for details). The magnitudes (A_0 for the lowest mode and A_s for s-th mode, $s > 1$) of each power normalized mode shape function and power normalized mode shape functions are as followings

$$A_0 = \frac{2V_t}{\omega^3 R^2}\sqrt{\frac{V_t}{\pi\rho}}, \quad s=0, \tag{2.7}$$

$$A_s = \frac{1}{V_t Z_s \left|J_s(Z_s)\right|}\sqrt{\frac{2}{\pi\rho\omega\left|\xi\right|}}, \quad s>0, \tag{2.8}$$

$$u_\theta = \frac{1}{X}\sqrt{\frac{2}{\pi\rho V_t^3\left|1-\left(Z_s/X\right)^2\right|^{1/2}}}\begin{cases} \sqrt{2}\left(r/R\right), & s=0, \\ \dfrac{Z_1\left(Z_s\times\left(r/R\right)\right)}{\left|J_1\left(Z_s\right)\right|}, & s>0, \end{cases} \tag{2.9}$$

where X indicates normalized frequency parameter, $X = R\omega/V_t = K_0 R$.

2.1.2 Modal scattering analysis

The power normalized mode shape function is applied to scattering problem defined as shown in figure 2.2. A solid rod having a circular cross section with a discontinuity at $z = 0$ is considered. Radius of left part and right part are indicated

by R_l and R_r, respectively. The subscripts l and r refer to the left and right part of solid rod which will be used below in other variables. In this chapter, the case of $R_l > R_r$ will be considered. When number of modes N is considered, the scattering can be described by

$$\begin{bmatrix} b_{l1} \\ b_{l2} \\ \cdots \\ b_{lN} \\ b_{r1} \\ b_{r2} \\ \cdots \\ b_{rN} \end{bmatrix} = \begin{bmatrix} [S_{11}] & [S_{12}] \\ & \\ [S_{21}] & [S_{22}] \end{bmatrix} \begin{bmatrix} a_{l1} \\ a_{l2} \\ \cdots \\ a_{lN} \\ a_{r1} \\ a_{r2} \\ \cdots \\ a_{rN} \end{bmatrix}. \tag{2.10}$$

The second indexes of a and b, from 1 to N, indicate the mode number and each of the sub-matrices is an $N \times N$ matrix. When waves income from both sides, two boundary conditions must be satisfied at the step as following:

(a) for $r < R_r$, continuity of displacement and stress, and

(b) for $r > R_r$, surface traction is equal to zero.

Displacement u and stress T which will be suppress the coordinate suffixes θ and z, will be considered. The displacement and stress of incoming wave on the left side, u_l^a and T_l^a, can be expanded in eigenmodes,

$$\begin{aligned} u_l^a &= \sum_i a_{l,i} u_{l,i} \exp(-j\xi_{l,i} z), \\ T_l^a &= \sum_i T_{l,i} = -jc_{44} \sum_i \xi_{l,i} a_{l,i} u_{l,i} \exp(-j\xi_{l,i} z), \end{aligned} \tag{2.11}$$

where, $a_{l,i}$ indicates the amplitude of the i-th incoming mode incoming in the left part. The outgoing wave in the left part can be obtained similarly,

$$u_l^b = \sum_i b_{l,i} u_{l,i} \exp(j\xi_{l,i} z),$$
$$T_l^b = \sum_i T_{l,i} = jc_{44} \sum_i \xi_{l,i} b_{l,i} u_{l,i} \exp(j\xi_{l,i} z), \tag{2.12}$$

Incoming and outgoing waves in the right part can be written very similarly (omitted here). Now, boundary condition as mentioned before for the velocity and stress at $z = 0$ (step position) is applied such as

$$j\omega u_l^a + j\omega u_l^b = j\omega u_r^a + j\omega u_r^b \quad r < R_r, \tag{2.13}$$

$$T_l^a + T_l^b = \begin{cases} T_r^a + T_r^b, & r < R_r \\ 0, & r > R_r \end{cases}. \tag{2.14}$$

These equations are expanded in eigenmodes as followings

$$j\omega \sum_i a_{l,i} u_{l,i} + j\omega \sum_i b_{l,i} u_{l,i} = j\omega \sum_i a_{r,i} u_{r,i} + j\omega \sum_i b_{r,i} u_{r,i}, \quad r < R_{r,} \tag{2.15}$$

$$\begin{aligned} & -jc_{44} \sum_i \xi_{l,i} a_{l,i} u_{l,i} + jc_{44} \sum_i \xi_{l,i} b_{l,i} u_{l,i} \\ & = \begin{cases} jc_{44} \sum_i \xi_{r,i} a_{r,i} u_{r,i} - jc_{44} \sum_i \xi_{r,i} b_{r,i} u_{r,i}, & r < R_r, \\ 0, & r < R_r. \end{cases} \end{aligned} \tag{2.16}$$

Equation (2.15) is multiplied by $-\frac{1}{2} T_{r,m} = \frac{1}{2} jc_{44} \xi_{r,m} u_{r,m}$ where $T_{r,m}$ is the relevant stress component of mode m in the right part. This party will be integrated over the cross section $0 < r < R_r$ after complex conjugated;

$$\begin{aligned} & \sum_i \pi c_{44} \omega \xi_{r,m} a_{l,i}^* \int_0^{R_r} u_{l,i} u_{r,m} r dr + \sum_i \pi c_{44} \omega \xi_{r,m} b_{l,i}^* \int_0^{R_r} u_{l,i} u_{r,m} r dr \\ & = \sum_i \pi c_{44} \omega \xi_{r,m} a_{r,i}^* \int_0^{R_r} u_{r,i} u_{r,m} r dr + \sum_i \pi c_{44} \omega \xi_{r,m} b_{r,i}^* \int_0^{R_r} u_{r,i} u_{r,m} r dr. \end{aligned} \tag{2.17}$$

By complex conjugating and adjusting $Q_{r,m} = \xi_{r,m} / K_0$, the normalized wave number, equation (2.17) can be represented

$$\begin{aligned} &\sum_i \pi c_{44} \omega Q_{r,m}^* a_{l,i} \int_0^{R_r} u_{l,i} u_{r,m} r dr + \sum_i \pi c_{44} \omega Q_{r,m}^* b_{l,i} \int_0^{R_r} u_{l,i} u_{r,m} r dr \\ &= \sum_i \pi c_{44} \omega Q_{r,m}^* a_{r,i} \int_0^{R_r} u_{r,i} u_{r,m} r dr + \sum_i \pi c_{44} \omega Q_{r,m}^* b_{r,i} \int_0^{R_r} u_{r,i} u_{r,m} r dr. \end{aligned} \tag{2.18}$$

This equation can be changed to

$$Q_{r,m}^* \sum_i L_{im} a_{l,i} + Q_{r,m}^* \sum_i L_{im} b_{l,i} = P_{r,m}^* a_{r,m} + P_{r,m}^* b_{r,m}, \tag{2.19}$$

by introducing L_{im},

$$L_{im} = \pi c_{44} \omega K_0 \int_0^{R_r} u_{l,i} u_{r,m} r dr = \pi \rho V_t \omega^2 \int_0^{R_r} u_{l,i} u_{r,m} r dr, \tag{2.20}$$

the real overlap integral. Similar formulas for equation (2.16), multiplying $-\frac{1}{2} v_{l,m}^* = \frac{1}{2} j\omega u_{l,m}$ and integrating over $0 < r < R_l$, are applied which yield

$$-P_{l,m} a_{l,m} + P_{l,m} b_{l,m} = \sum_i Q_{r,i} L_{mi} a_{r,i} - \sum_i Q_{r,i} L_{mi} b_{r,i}. \tag{2.21}$$

Equations (2.19) and (2.21) are used to find the scattering parameters of stepped rod system after dividing the equation (2.19) by $P_{r,m}^*$:

$$\begin{aligned} &\left|Q_{r,m}\right| \sum_i L_{im} b_{l,i} - b_{r,m} = -\left|Q_{r,m}\right| \sum_i L_{im} a_{l,i} - a_{r,m}, \\ &P_{l,m} b_{l,m} + \sum_i Q_{r,i} L_{mi} b_{r,i} = P_{l,m} a_{l,m} + \sum_i Q_{r,i} L_{mi} a_{r,i}. \end{aligned} \tag{2.22}$$

Note that b can be determined by solving equation (2.22) which is infinite set of linear equation when *a*'s are known, the magnitude of each incident wave mode. 2*N*

equations should be considered to determine 2*N* mode, *N*-th mode for outgoing wave toward both sides. For *N*=3 case as an example, equation (2.22) can be written

$$\begin{bmatrix} |Q_{r,1}|L_{11} & |Q_{r,1}|L_{21} & |Q_{r,1}|L_{31} & -1 & 0 & 0 \\ |Q_{r,2}|L_{12} & |Q_{r,2}|L_{22} & |Q_{r,2}|L_{32} & 0 & -1 & 0 \\ |Q_{r,3}|L_{13} & |Q_{r,3}|L_{23} & |Q_{r,3}|L_{33} & 0 & 0 & -1 \\ P_{l,1} & 0 & 0 & Q_{r,1}L_{11} & Q_{r,1}L_{12} & Q_{r,1}L_{13} \\ 0 & P_{l,2} & 0 & Q_{r,2}L_{21} & Q_{r,2}L_{22} & Q_{r,2}L_{23} \\ 0 & 0 & P_{l,3} & Q_{r,3}L_{31} & Q_{r,3}L_{32} & Q_{r,3}L_{33} \end{bmatrix} \begin{bmatrix} b_{l,1} \\ b_{l,2} \\ b_{l,3} \\ b_{r,1} \\ b_{r,2} \\ b_{r,3} \end{bmatrix}$$

$$= \begin{bmatrix} -|Q_{r,1}|L_{11} & -|Q_{r,1}|L_{21} & -|Q_{r,1}|L_{31} & 1 & 0 & 0 \\ -|Q_{r,2}|L_{12} & -|Q_{r,2}|L_{22} & -|Q_{r,2}|L_{32} & 0 & 1 & 0 \\ -|Q_{r,3}|L_{13} & -|Q_{r,3}|L_{23} & -|Q_{r,3}|L_{33} & 0 & 0 & 1 \\ P_{l,1} & 0 & 0 & Q_{r,1}L_{11} & Q_{r,1}L_{12} & Q_{r,1}L_{13} \\ 0 & P_{l,2} & 0 & Q_{r,2}L_{21} & Q_{r,2}L_{22} & Q_{r,2}L_{23} \\ 0 & 0 & P_{l,3} & Q_{r,3}L_{31} & Q_{r,3}L_{32} & Q_{r,3}L_{33} \end{bmatrix} \begin{bmatrix} a_{l,1} \\ a_{l,2} \\ a_{l,3} \\ a_{r,1} \\ a_{r,2} \\ a_{r,3} \end{bmatrix}. \quad (2.23)$$

2.2 Stepped pipe scattering theory

2.2.1 Power normalized mode shape function

Stepped pipe scattering theory can be obtained by very similar procedure with stepped rod problem reviewed in section 2.1 because rod and pipe show analogous physical phenomena. The biggest different part is mode shape function as showed before in equation (2.2). In the pipe problem, mode shape function can be written as following [33]

$$u_\theta = A_0 K_0^2 r, \qquad s = 0, \tag{2.24}$$

$$u_\theta = A_s k_r J_1(k_r r) + B_s k_r Y_1(k_r r), \qquad s > 0. \tag{2.25}$$

Equation (2.24) and (2.25) denote the lowest torsional wave mode and higher torsional modes, respectively. Where J_i and Y_i denote first and second kind of the Bessel function for order *i*. The next step is to induce power normalized mode shape function like equation (2.9). As with the previous course, the condition represented in equation (2.6) will be applied to equation (2.5) to obtain power normalized mode shape function of a pipe structure. In this section a pipe having inner radius R_i and outer radius R is considered. For the lowest torsional wave mode, total power P can be written as following using equation (2.24)

$$P = \pi\omega\mu\xi \int_{R_i}^{R} u_{\theta,s} u_{\theta,s} r dr = \pi\omega\mu\xi \int_{R_i}^{R} {A_0}^2 {K_0}^4 r^3 dr. \tag{2.26}$$

Note that the lowest torsional wave mode is always propagating mode, so that total power P always have the value of 1. From that the equation (2.26) always has the value of 1, one can determine constant A_0 of power normalized mode shape function of the first torsional wave mode as following equations

$$\pi\rho {V_t}^3 {A_0}^2 {K_0}^6 \frac{1}{4}\left(R^4 - R_i^4\right) = 1, \tag{2.27}$$

$${A_0}^2 = \frac{4P}{\pi\rho {V_t}^3 {K_0}^6 \left(R^4 - R_i^4\right)}, \tag{2.28}$$

$$A_0 = \frac{2}{{V_t}{K_0}^3} \frac{1}{\sqrt{\pi\rho V_t \left(R^4 - R_i^4\right)}}. \tag{2.29}$$

For the second and higher torsional wave mode, equation (2.25) looks like it has two unknown coefficients, the number of unknown can be reduced by applying traction free boundary condition at $r = R_i$ and R. Starting with stress component $T_{r\theta}$ to apply traction free boundary condition, $T_{r\theta}$ can be written

$$T_{r\theta} = \mu r \frac{\partial}{\partial r}\left(\frac{u_\theta}{r}\right) = \mu\left(-\frac{u_\theta}{r} + \frac{\partial u_\theta}{\partial r}\right). \tag{2.30}$$

By adjusting derivative of Bessel function as following

$$\frac{d}{dx} Z_\nu(x) = \frac{1}{2}\left[Z_{\nu-1}(x) - Z_{\nu+1}(x)\right], \tag{2.31}$$

where Z denotes the first kind Bessel function for the order ν, equation (2.30) can be represented

$$\begin{aligned} &A_s \frac{\mu r}{2}\left(-r k_r^{\,2} J_0(k_r r) + k_r J_1(k_r r) + r k_r^{\,2} J_2(k_r r)\right) \\ &+ B_s \frac{\mu r k_r}{2}\left(-r k_r Y_0(k_r r) + Y_1(k_r r) + r k_r Y_2(k_r r)\right) \end{aligned}. \tag{2.32}$$

And equation (2.32) can be written

$$T_{r\theta} = \mu r^2 k_r^{\,2}\left[A_s J_2(k_r r) + B_s Y_2(k_r r)\right] \tag{2.33}$$

by adjusting characteristic of Bessel function,

$$2\nu Z_\nu(x) = x[Z_{\nu-1}(x) + Z_{\nu+1}(x)]. \tag{2.34}$$

Two linear equation for A_s and B_s can be obtained by applying boundary condition at the inner and outer surface; $T_{r\theta} = 0 \quad (r = R_i,\ R)$, as followings

$$\begin{aligned} A_s J_2(k_r R_i) + B_s Y_2(k_r R_i) &= 0, \\ A_s J_2(k_r R) + B_s Y_2(k_r R) &= 0, \end{aligned} \tag{2.35}$$

which can be represented in matrix form

$$\begin{bmatrix} J_2(k_r R_i) & Y_2(k_r R_i) \\ J_2(k_r R) & Y_2(k_r R) \end{bmatrix} \begin{bmatrix} A_s \\ B_s \end{bmatrix} = 0 . \tag{2.36}$$

To satisfy equation (2.36) determinant of the matrix in the left part should be zero which means characteristic equation. And A_s and B_s are dependent which are satisfying following condition

$$J_2(k_r R_i) A_s + Y_2(k_r R_i) B_s = 0 . \tag{2.37}$$

Finally, mode shape function for the higher torsional mode can be expressed with one coefficient A_s

$$u_\theta = -A_s \left[k_r J_1(k_r r) - \left(J_2(k_r R_i) / Y_2(k_r R_i) \right) k_r Y_1(k_r r) \right] \tag{2.38}$$

Now the coefficient A_s should be defined to satisfy that total power becomes 1 or -j for propagating mode or non-propagating mode respectively. Similarly with equation (2.26)-(2.29) total power P can be obtained using equation (2.38). To this end, integral shown in following equation should be solved.

$$\int_{R_i}^{R} u_{\theta,s} u_{\theta,s} r dr = A_s^{\,2} k_r^{\,2} \int_{R_i}^{R} \left[Y_2(k_r R_i) J_1(k_r r) - J_2(k_r R_i) k_r Y_1(k_r r) \right]^2 r dr . \tag{2.39}$$

This integral can be solved using established integral table of Bessel functions [34, 35] as following

$$\int^{z} C_v^{\,2}(kt)t\,dt = \frac{1}{2}z^2\left\{C_v^{\,2}(kz) - C_{v-1}(kz)C_{v+1}(kz)\right\} \tag{2.40}$$

where C_v is a cylindrical function such as

$$C_v(z) = AJ_v(z) + BY_v(z)\,. \tag{2.41}$$

Now, equation (2.39) can be solved as

$$A_s^{\,2}k_r^{\,2}\left[\frac{1}{2}r^2\left\{C_1^{\,2}(k_r r) - C_0(k_r r)C_2(k_r r)\right\}\right]_{R_i}^{R}. \tag{2.42}$$

And by substituting the integration constants and introducing C_n which denotes

$$C_n(k_r r) = Y_2(k_r R_i)J_n(k_r r) - J_2(k_r R_i)Y_n(k_r r)\,, \tag{2.43}$$

with a condition of

$$C_2(k_r R_i) = C_2(k_r R) = 0\,, \tag{2.44}$$

equation (2.42) can be written

$$\frac{1}{2}A_s^{\,2}k_r^{\,2}\left[R^2C_1^{\,2}(k_r R) - R_i^{\,2}C_1^{\,2}(k_r R_i)\right]. \tag{2.45}$$

Thus, total power P can be written

$$P = \frac{1}{2}\pi\omega\mu\xi A_s^{\,2}k_r^{\,2}\left[R^2C_1^{\,2}(k_r R) - R_i^{\,2}C_1^{\,2}(k_r R_i)\right]. \tag{2.46}$$

As mentioned before, for normalization of each torsional mode, the total power P should be 1 or $-j$ for propagating or non-propagating mode. Therefore magnitude of each torsional mode A_s should be

$$A_s = \frac{1}{V_t k_r}\sqrt{\frac{2}{\pi\omega\rho\left|\xi\left[R^2 C_1^{\,2}(k_r r) - R_i^{\,2} C_1^{\,2}(k_r R_i)\right]\right|}}\,. \qquad (2.47)$$

The power normalized displacement function for the higher torsional modes, therefore, are given by

$$u_\theta = \frac{1}{V_t}\sqrt{\frac{2}{\pi\omega\rho\left|\xi\left[R^2 C_1^{\,2}(k_r R) - R_i^{\,2} C_1^{\,2}(k_r R_i)\right]\right|}}\times \left[Y_2(k_r R_i)J_1(k_r r) - J_2(k_r R_i)k_r Y_1(k_r r)\right] \qquad (2.48)$$

Finally, the power normalized mode shape function can be found that can be written

$$u_\theta = \begin{cases} \dfrac{2}{\sqrt{\pi\rho V_t^{\,3} K_0^{\,2}(R^4 - R_i^{\,4})}}\, r & s = 0 \\ \dfrac{1}{V_t}\sqrt{\dfrac{2}{\pi\omega\rho\left|\xi\left[R^2 C_1^{\,2}(k_r R) - R_i^{\,2} C_1^{\,2}(k_r R_i)\right]\right|}}\times \left[Y_2(k_r R_i)J_1(k_r r) - J_2(k_r R_i)k_r Y_1(k_r r)\right] & s > 0 \end{cases} \qquad (2.49)$$

To verify obtained power normalized mode shape function represented in equation (2.49) mode shape of the second and fifth mode are shown in figure 2.3. Mode shapes in an aluminum pipe having 70-mm diameter and 13-mm thickness are considered. For comparison, commercial tool DISPERSE [36] is used. Each curve in figure 2.3 was normalized with respect to its own maximum value. From the figure 2.3 it is confirmed that driven power normalized mode shape function is appropriate.

2.2.2 Modal scattering analysis

The power normalized mode shape function is now used to find scattering matrix for a stepped pipe problem shown in figure similarly with section 2.1.2. A schematic of stepped pipe problem is shown in figure 2.4. Outer radius of the left part and right part are denoted R_l and R_r, respectively. For convenience, a stepped pipe which has the same inner radius R_i will be considered in this section. Every procedure to obtain scattering matrix is the same with the section 2.1.2, established in the previous paper, except power normalized mode shape function and integral section. The power normalized mode shape function is shown in equation (2.49) and integral section is changed starting from R_i not zero in the rod case. Thus the final result shows the same thing in equation (2.23) only the differences in definition of $L_{im,}$

$$L_{im} = \pi\rho V_t \omega^2 \int_{R_i}^{R_r} u_{l,i} u_{r,m} r dr \ . \tag{2.50}$$

The integral section of P is also changed, but the values of P are always 1 or $-j$ for the propagating modes or non-propagating modes.

To obtain frequency response of the stepped pipe scattering, examples for aluminum pipes having 22-mm inner radius R_i and 35-mm outer radius of the left part R_l, three cases of outer radius of the right part R_r = 32, 29, and 26 mm, were considered. For an incident first torsional wave mode in a left part, magnitude of the reflected wave modes were calculated. Re-expressed it as the form in equation (2.23),

$$\begin{bmatrix} |Q_{r,1}|L_{11} & |Q_{r,1}|L_{21} & |Q_{r,1}|L_{31} & -1 & 0 & 0 \\ |Q_{r,2}|L_{12} & |Q_{r,2}|L_{22} & |Q_{r,2}|L_{32} & 0 & -1 & 0 \\ |Q_{r,3}|L_{13} & |Q_{r,3}|L_{23} & |Q_{r,3}|L_{33} & 0 & 0 & -1 \\ P_{l,1} & 0 & 0 & Q_{r,1}L_{11} & Q_{r,1}L_{12} & Q_{r,1}L_{13} \\ 0 & P_{l,2} & 0 & Q_{r,2}L_{21} & Q_{r,2}L_{22} & Q_{r,2}L_{23} \\ 0 & 0 & P_{l,3} & Q_{r,3}L_{31} & Q_{r,3}L_{32} & Q_{r,3}L_{33} \end{bmatrix} \begin{bmatrix} b_{l,1} \\ b_{l,2} \\ b_{l,3} \\ b_{r,1} \\ b_{r,2} \\ b_{r,3} \end{bmatrix}$$
$$= \begin{bmatrix} -|Q_{r,1}|L_{11} & -|Q_{r,1}|L_{21} & -|Q_{r,1}|L_{31} & 1 & 0 & 0 \\ -|Q_{r,2}|L_{12} & -|Q_{r,2}|L_{22} & -|Q_{r,2}|L_{32} & 0 & 1 & 0 \\ -|Q_{r,3}|L_{13} & -|Q_{r,3}|L_{23} & -|Q_{r,3}|L_{33} & 0 & 0 & 1 \\ P_{l,1} & 0 & 0 & Q_{r,1}L_{11} & Q_{r,1}L_{12} & Q_{r,1}L_{13} \\ 0 & P_{l,2} & 0 & Q_{r,2}L_{21} & Q_{r,2}L_{22} & Q_{r,2}L_{23} \\ 0 & 0 & P_{l,3} & Q_{r,3}L_{31} & Q_{r,3}L_{32} & Q_{r,3}L_{33} \end{bmatrix} \begin{bmatrix} 1 \\ 0 \\ 0 \\ 0 \\ 0 \\ 0 \end{bmatrix} . \quad (2.51)$$

Note that only $a_{l,1}$ is 1 and all the other a's are zero to express that only the first torsional mode in the left part propagate to the step in a pipe. Reflection and transmission coefficients of each wave modes can be obtained respectively from b_l's and b_r's represented in a matrix form as following

$$\begin{bmatrix} b_{l,1} \\ b_{l,2} \\ b_{l,3} \\ b_{r,1} \\ b_{r,2} \\ b_{r,3} \end{bmatrix} = M_b^{-1} M_a \begin{bmatrix} 1 \\ 0 \\ 0 \\ 0 \\ 0 \\ 0 \end{bmatrix} . \quad (2.52)$$

Here, M_a and M_b denote the matrix in the right side and right side in equation (2.51) respectively. The results of reflection coefficients for the first and second torsional mode, $b_{l,1}$ and $b_{l,2}$, are shown in figure 2.5 and 2.6. From figure 2.5, reflection coefficients of the first torsional mode show that reflection from stepped pipe occurs more when the depth of step becomes larger. This is reasonable inferred

from the fact that as the size of the defect is large reflection is large. The resonance effects at the cut-off frequencies are also observe. In figure 2.5, peaks near 120 kHz and 230 kHz occur which are first and second cut-off frequency of the 13-mm thickness pipe. At the cut-off frequency cut-off mode diverges, this makes resonance phenomena. In figure 2.6, because the cut-off frequency of the second torsional mode is near 120 kHz, reflection coefficients under cut-off frequency are set to be zero.

2.3 Validation with numerical simulation

2.3.1 Numerical analysis

To verify proposed stepped pipe scattering theory, numerical simulation will be carried out. COMSOL multiphysics [37] was used for the numerical model represented in figure 2.8 for R_i = 22 mm and R_l = 35 mm. Here, partial differential equation for the axisymmetric torsional wave problem,

$$\frac{\partial^2 u_\theta}{\partial r^2}+\frac{1}{r}\frac{\partial u_\theta}{\partial r}-\frac{u_\theta}{r^2}+\frac{\partial^2 u_\theta}{\partial z^2}=\frac{1}{V_t^2}\frac{\partial^2 u_\theta}{\partial t^2}, \tag{2.53}$$

were solved by PDE module in COMSOL. Gabor pulse, which is good for energy concentration with respect to a specific frequency, was used as an input pulse with 200-kHz center frequency at the excitation line. The shape of input Gabor pulse and its Fourier transform are shown in figure 2.9. Time transient finite element

analyses were carried out with respect to 1-mm maximum mesh size and 0.05-μs time interval. To generate only the lowest torsional mode, distributed loading was excited at the excitation line in figure 2.8. This distribution is formed linear function which is the mode shape of the first torsional wave mode. When the specific mode shape is loaded, that mode can be generated alone virtually. As an example 6-mm step depth case is considered here, and its measured signal is presented in figure 2.10. The signal is normalized by the magnitude of the input signal (even not shown in the figure). Note that the excited frequency of 200 kHz is located between the first and the second cut-off frequency (see figure 2.7), the first and second torsional mode would be reflected. In the figure 2.10, a sharp signal is the first torsional mode and a spread one is the second one. Because the second torsional mode has dispersive property otherwise the first torsional mode is non-dispersive.

Now, let us back to the results of the stepped pipe scattering theory. Reflection coefficients for the 6-mm step depth case are shown as dotted lines in figure 2.6 and 2.7. These results should be compared with the results obtained by numerical analyses like one represented in figure 2.10. The main differences occur because the results obtained by scattering theory are under time-harmonic assumption. Otherwise, the results obtained numerically are based on time transient analysis which uses Gabor pulse as an input signal. Thus the method to make reflection signal from scattering theory should be applied. It is possible by inverse Fourier transform after multiplying FFT result of input pulse in the Fourier domain. Figure 2.11 shows result of multiplying frequency response from stepped pipe represented in figure 2.5 (result of the first torsional mode) and FFT of input Gabor pulse

represented in figure 2.9(b). Reflected signal can be calculated after inverse Fourier transform of this, and the results of the first and second torsional wave modes are shown in figure 2.12. The numbers expressed by T_1 and T_2 denote reflection coefficient of the first and second torsional wave modes, respectively. Note that these signals are reflected signals at the reflective moment.

2.3.2 Signal processing: dispersion compensation

Let us start with the results of the numerical simulation represented in figure 2.10. Because the second torsional mode has dispersive property, second mode signal shows increasing aspect. Therefore judgment of reflection coefficient of the second torsional mode is difficult. Moreover dispersive signal changes its shape when propagating along a pipe. Generally magnitude of dispersive signal becomes smaller during propagation because of wave diffusion. Thus the method to compare magnitude of the dispersive signal; reflected second torsional mode here, to obtained signal from stepped pipe scattering theory represented in figure 2.12, should be employed. To this end, dispersion compensation method [31] which has been reported will be employed. Although the detailed procedure is well presented in [31], brief review will be shown from now on with some notation changes.

Let us assume there is measured guided wave mode of interest $u(x,t)$ excited from an input signal $f(t)$, where t and x is time and propagating distance of the guided wave respectively. $u(x,t)$ can be represented

$$u(x,t) = \int_{-\infty}^{\infty} F(\omega) e^{i(k(\omega)x - \omega t)} d\omega, \tag{2.54}$$

where, $k(\omega)$ is the wave number as a function of frequency ω and $F(\omega)$ is the Fourier transform of $f(t)$.

And there is $g(t)$, received time signal apart from transducer to *x*, which should be a function of propagation distance and compressed it dispersion. Now if one propagates $g(t)$ as *-x*, back propagating, dispersion compensated time signal $h(x)$ can be calculated;

$$h(x) = u(-x,0) = \int_{-\infty}^{\infty} G(\omega) e^{-ik(\omega)x} d\omega, \tag{2.55}$$

where $G(\omega)$ is the Fourier transform of $g(t)$. The integration variable ω should be change from ω to *k* using the relation;

$$\begin{aligned} d\omega &= v_{gr}(\omega) dk \\ \omega &= v_{ph}(\omega) k \end{aligned} \tag{2.56}$$

where v_{gr}, v_{ph} denote the group and phase velocities of the mode, respectively. Using equation (2.55), needs more numerical implementation, dispersion signal can be compressed if dispersion relation ($\omega - k$) is already known.

In this section, dispersion relation of an aluminum pipe is already known, dispersion compensation of obtained signal is possible. A clamped signal from original signal shown in figure 2.10 for the second torsional wave mode is represented in figure 2.13(a). This signal is compensated using equation (2.55) and

the result is shown in figure 2.13(b). The signals which are obtained by scattering theory and by numerical analysis after dispersion compensation are shown in figure 2.14 together. From the figure it is confirmed that dispersion compensation method works well and obtained signals from scattering theory and numerical analysis after dispersion compensation show good agreement.

2.3.3 Numerical validation

For numerical validation of proposed stepped pipe scattering theory, 2-dimensional time transient finite element analyses were carried out for the numerical mode explained in section 2.3.1 and figure 2.8. Depth of step is changed from 1 to 13 mm in 1-mm interval. Calculated reflection coefficients of the first and second torsional wave mode are represented in figure 2.15 in addition reflection coefficients obtained from scattering theory. Note that the results of the numerical simulation were obtained after dispersion compensation. At first, it is validated that the results of numerical simulation and scattering theory show good agreement from figure 2.15. Two reflected modes, the first and second torsional wave mode, show deferent aspect for change of step depth. The first mode shows increasing tendency, otherwise, reflection coefficient of the second mode grows up until 5-mm step depth and decreases. The results can be explained from the mode shapes of two torsional wave modes shown in figure 2.16. The mode shape of the first torsional mode is linear which has uniform sign, whereas that of the second one consists of function which changes sign on the way. This difference of two modes causes different reflection coefficient patterns

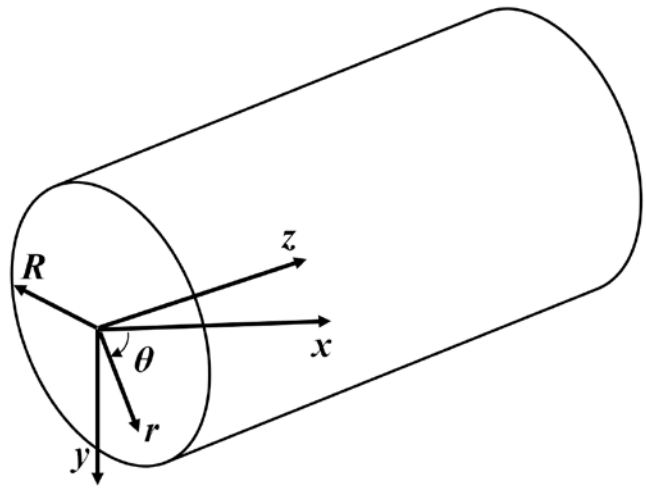

Figure 2. 1. Definition of the cylindrical coordinate system

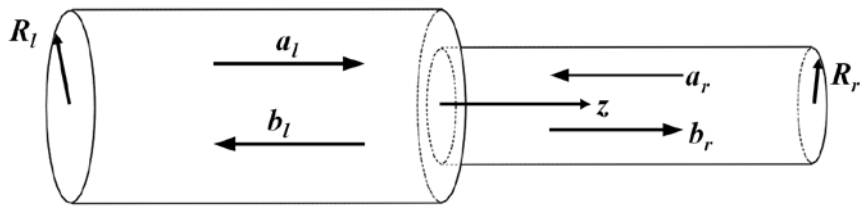

Figure 2. 2. Definition of geometry of stepped rod. *a* and *b* denote incoming and outgoing waves, and *l* and *r* mean left and right part of stepped rod respectively

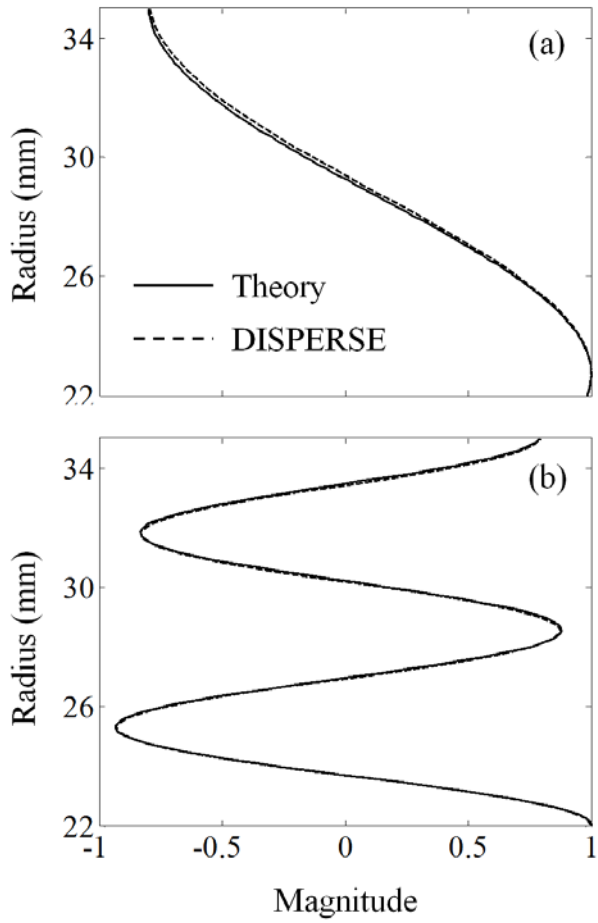

Figure 2. 3. Mode shapes of the (a) second and (b) fifth torsional wave modes obtained by the proposed equation (1.49) and commercial tool DISPERSE which are denoted by solid and dotted line, respectively.

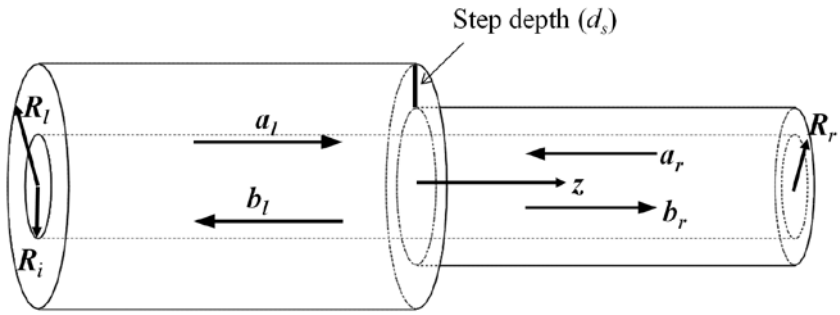

Figure 2. 4. Definition of a stepped pipe for a stepped pipe scattering theory having the same inner radius R_i.

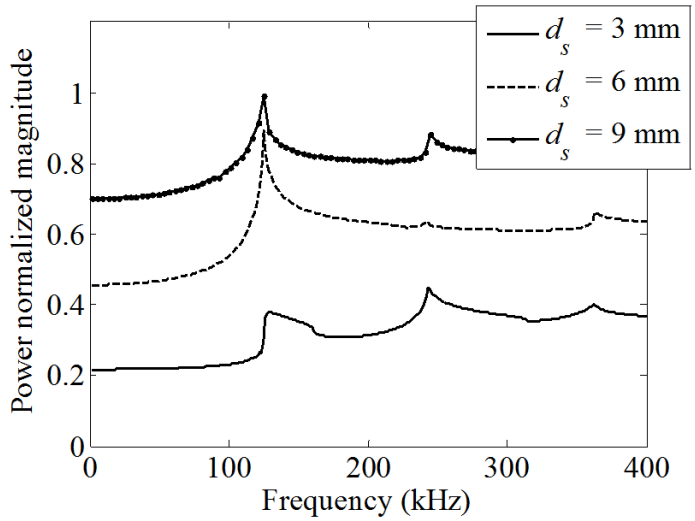

Figure 2. 5. Frequency response of the reflected first torsional wave mode for the incident first torsional wave mode at the stepped pipe having step depth d_s = 3, 6 and 9 mm.

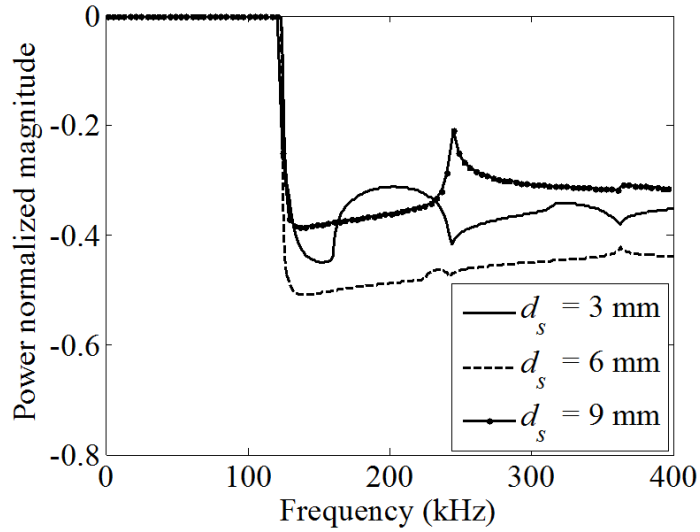

Figure 2. 6. Frequency response of the reflected second torsional wave mode for the incident first torsional wave mode at the stepped pipe having step depth d_s = 3, 6 and 9 mm.

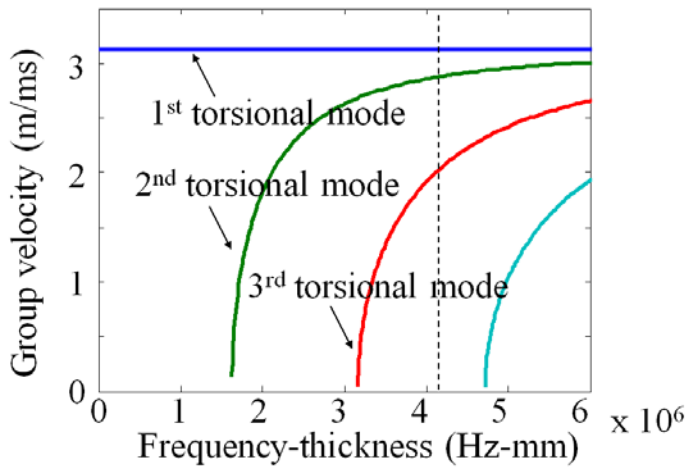

Figure 2. 7. Dispersion relation of the torsional waves in an aluminum pipe.

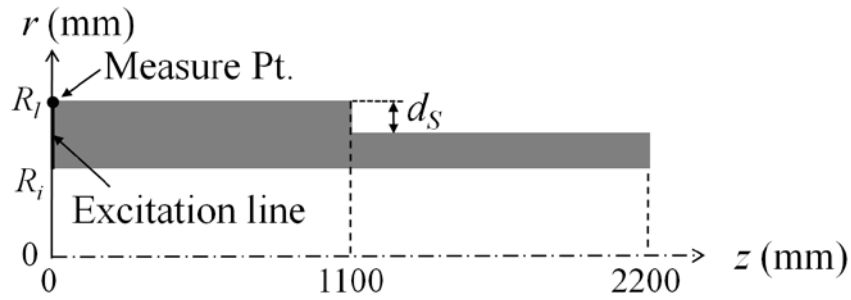

Figure 2. 8. Schematics of FEM model for stepped pipe scattering problem.

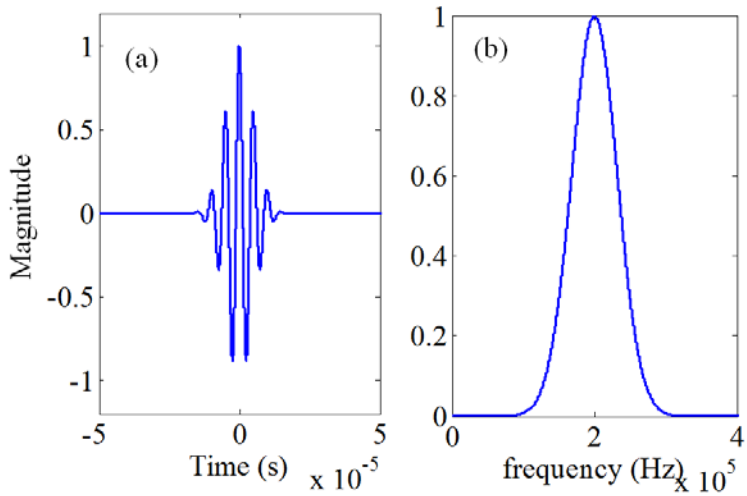

Figure 2. 9. (a) Shape of Gabor pulse with 200-kHz center frequency and (b) its Fourier transform result.

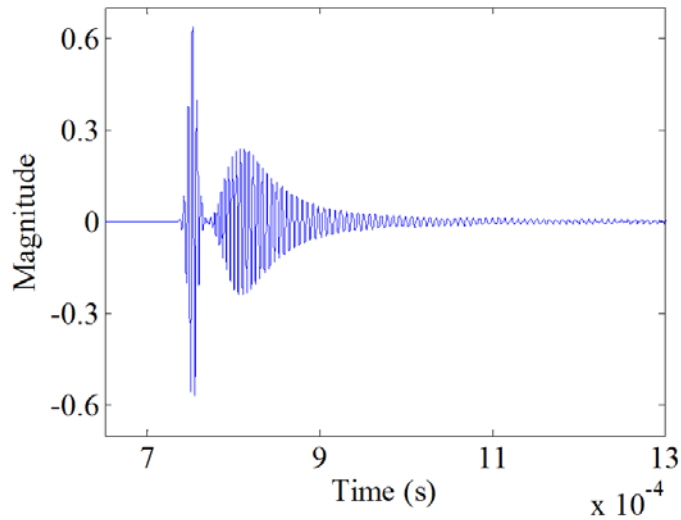

Figure 2. 10. Result of the finite element analysis for the model in figure 2.8 with d_s = 6 mm. The signal was normalized by the magnitude of the input signal.

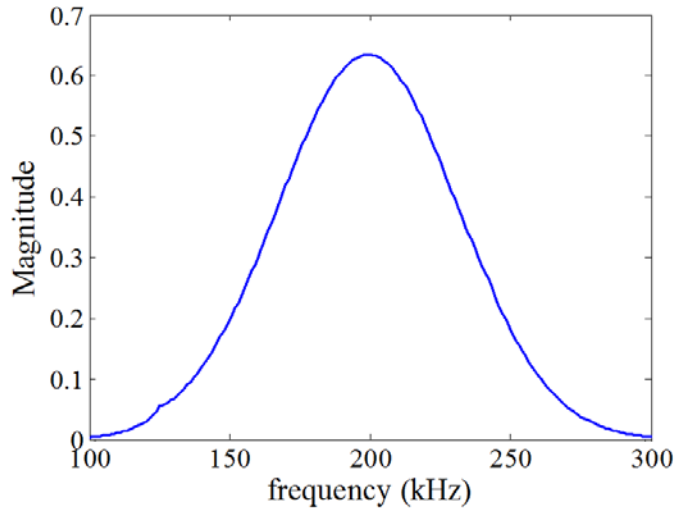

Figure 2. 11. Result of multiplying frequency response from stepped pipe represented in figure 2.5 (result of the first torsional mode) and FFT of input Gabor pulse represented in figure 2.9(b).

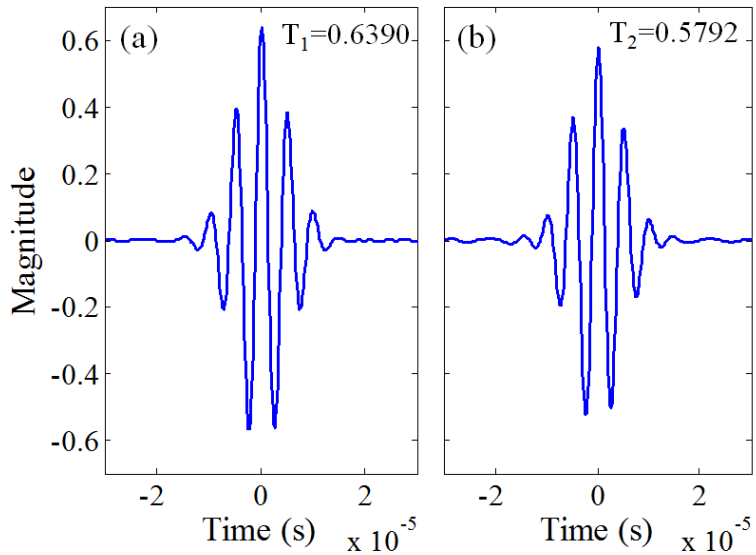

Figure 2. 12. Reflected signals of the (a) first and (b) second torsional wave mode calculated by inverse Fourier transform for the product of stepped pipe FRF results and FFT of the input Gabor pulse. An example is shown in figure 2.11 for the first torsional wave case.

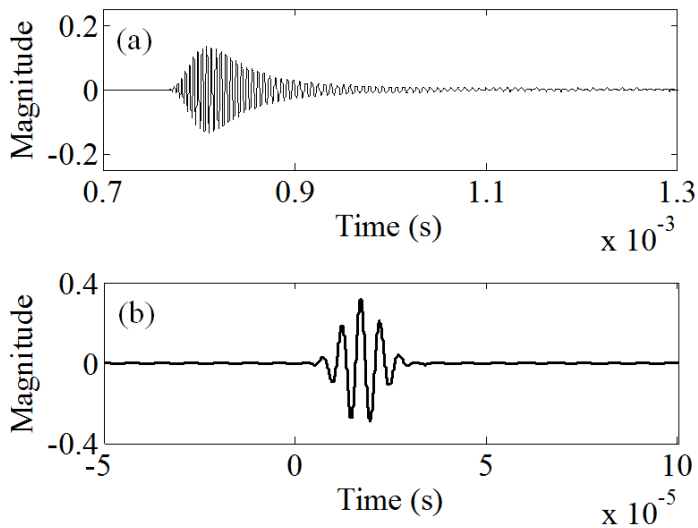

Figure 2. 13. (a) A clamped second torsional wave signal from calculated signal shown in figure 2.10. (b) Dispersion compensated signal of (a).

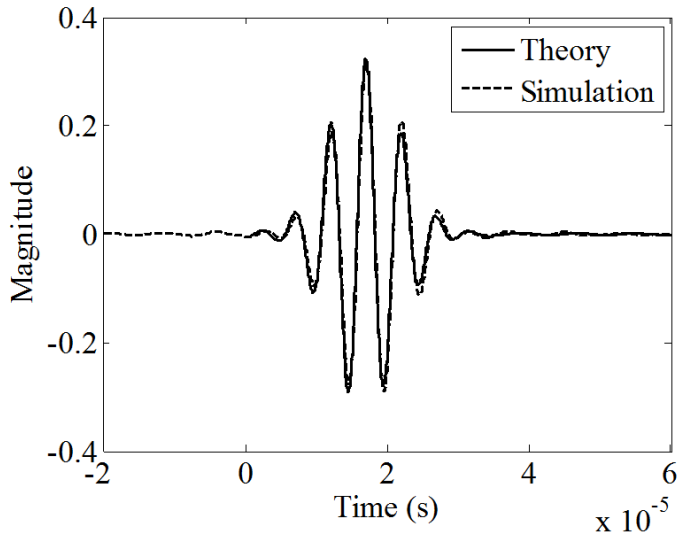

Figure 2. 14. The signals which are obtained by (a) scattering theory and by (b) numerical simulation. The result of (b) are obtained after dispersion compensation.

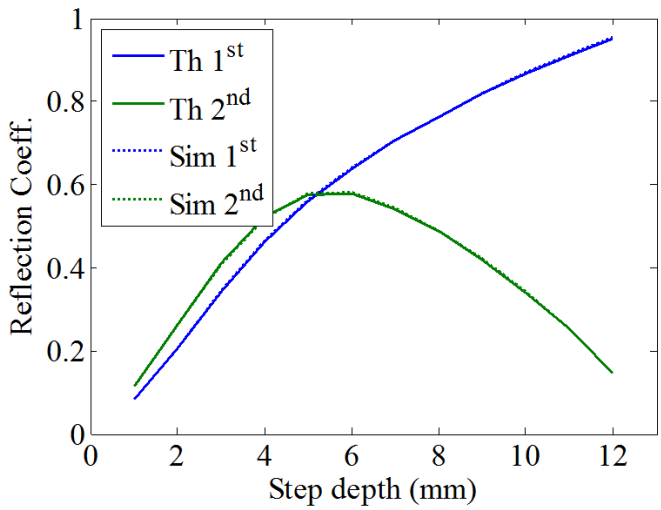

Figure 2. 15. Reflection coefficients of the first and second torsional wave modes which are obtained by scattering theory (represented as Th) and numerical simulation (represented as Sim).

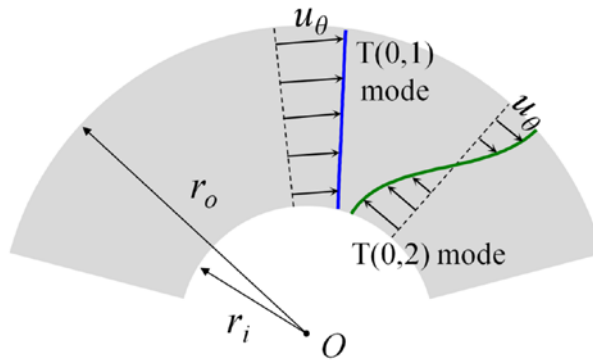

Figure 2. 16. Mode shape in the thickness direction for the first and second torsional wave modes.

CHAPTER 3.

Scattering analysis from an axisymmetric notch defect in a pipe

In this chapter, stepped pipe scattering theory proposed in chapter 2 will be expended to axisymmetric notch scattering case. To this end multiple scattering of the stepped pipe scattering theory will be carried out in section 3.1. The results will be validated by numerical simulation in section 3.2. Finally, axisymmetric notch defect theory will be validated experimentally in section 3.3. The proposed axisymmetric notch scattering theory will be used as a reference to characterize size of notch defect. There are also some researches which are concerned with scattering of guided wave such as hybrid semi-analytical finite element methods [38-41] numerical eigen mode extraction method [42-48]. In this research, through dispersion compensation process of measured signal, notch size estimation is possible by directly comparing with the proposed scattering theory.

3.1 Axisymmetric notch scattering theory

Definition of an axisymmetric notch defect problem is shown in figure 3.1(a) for a pipe having outer radius of R and inner radius of R_i. Because a target notch is axisymmetric, two variables; notch depth (d_N) and length (L_N), can define notch

geometry. Scattering at the notch defect can be treated multiple scattering of stepped pipe as shown in figure 3.1(b). Before starting details about axisymmetric notch scattering, two matrices; scattering matrix *S* and propagation matrix *P*, are introducing as followings;

$$[S]=[M_b]^{-1}[M_a] \tag{3.1}$$

$$[P]=\begin{bmatrix} 0 & 0 & e^{-jK_0L} & 0 \\ 0 & 0 & 0 & e^{-j\xi_1 L} \\ e^{-jK_0L} & 0 & 0 & 0 \\ 0 & e^{-j\xi_1 L} & 0 & 0 \end{bmatrix}, \tag{3.2}$$

where M_a and M_b are defined in equation (2.52) and *P* is an example for the case of two modes consideration. Total reflected signal can be expressed in the synthesis of multiple scattered signals. Here, the process of obtaining the first and second reflected signals will be presented. The first reflected signal can be easily obtained using equation (2.52), note that it is the same with reflection of the stepped pipe scattering problem;

$$[S]\times\begin{Bmatrix}\vec{a}_l \\ \vec{a}_r\end{Bmatrix}=\begin{Bmatrix}\vec{b}_{l\_\text{step1}} \\ \vec{b}_{r\_\text{step1}}\end{Bmatrix}, \tag{3.3}$$

here, $\vec{b}_{l\_\text{step1}}$ is reflection coefficients vector of the first reflected signal;

$$\vec{b}_{l\_\text{step1}}=\vec{b}_{1\text{st\_ref}}\,. \tag{3.4}$$

Note that every components of the input wave vectors $\vec{a}_l$ and $\vec{a}_r$ has zero value except the first component of $\vec{a}_l$ to express incident first torsional wave only in

the left. Transmitted wave vector $\vec{b}_{r\_\text{step1}}$ is used input vector from left in the next step; propagation step. Phase change caused by propagation in the notch is considered in this step using propagation matrix *P*;

$$[P]\times\begin{Bmatrix}\vec{a}_l=\vec{b}_{r\_\text{step1}}\\ \vec{a}_r=0\end{Bmatrix}=\begin{Bmatrix}\vec{b}_{l\_\text{step2}}=0\\ \vec{b}_{r\_\text{step2}}\end{Bmatrix}. \tag{3.5}$$

Input vector in right part, $\vec{a}_r$, should be zero for the definition of the propagation form left to right. In addition, reflection to the left direction, $\vec{b}_{l\_\text{step2}}$, is also zero. This step2 can be expressed simply;

$$\left[\tilde{P}\right]\times\left\{\vec{b}_{r\_\text{step1}}\right\}=\left\{\vec{b}_{r\_\text{step2}}\right\}. \tag{3.6}$$

where $\tilde{P}$ denotes

$$\tilde{P}=\begin{bmatrix}0 & e^{-jK_0L}\\ e^{-j\xi_1L} & 0\end{bmatrix} \tag{3.7}$$

which is also an example of the two mode case. The propagating wave is now reflected and transmitted at the right edge. Here, stepped pipe has thin left part and thick right part which is opposite to step1. The case that incident wave from the left reflects to the left direction should be considered. To this end scattering matrix S should be obtained again. To avoid this, the direction of stepped pipe in step3 is changed; for the incident wave from the right, reflected wave to the right direction will be considered in a stepped pipe having thick left part and thin right part. In a matrix form it can be written

$$[S]\times\begin{Bmatrix}\vec{a}_l = 0\\ \vec{a}_r = \vec{b}_{r\_\text{step2}}\end{Bmatrix}=\begin{Bmatrix}\vec{b}_{l\_\text{step3}}\\ \vec{b}_{r\_\text{step3}}\end{Bmatrix}. \tag{3.8}$$

Note that $\vec{b}_{l\_\text{step3}}$ and $\vec{b}_{r\_\text{step3}}$ denote transmitted and reflected waves, respectively. The transmitted wave is not interest in this research, reflected wave will be used in the next step. Step4 is propagating step which is similar to step2 but only the direction is changed as from right to left for the incident wave of $\vec{b}_{r\_\text{step3}}$;

$$[P]\times\begin{Bmatrix}\vec{a}_l = 0\\ \vec{a}_r = \vec{b}_{r\_\text{step3}}\end{Bmatrix}=\begin{Bmatrix}\vec{b}_{l\_\text{step4}}\\ \vec{b}_{r\_\text{step4}} = 0\end{Bmatrix}. \tag{3.9}$$

The final step, step5, $\vec{b}_{l\_\text{step4}}$ is incident wave from right;

$$[S]\times\begin{Bmatrix}\vec{a}_l = 0\\ \vec{a}_r = \vec{b}_{l\_\text{step4}}\end{Bmatrix}=\begin{Bmatrix}\vec{b}_{l\_\text{step5}}\\ \vec{b}_{r\_\text{step5}}\end{Bmatrix}. \tag{3.10}$$

The transmitted signal $\vec{b}_{l\_\text{step5}}$ becomes the second reflected signal;

$$\vec{b}_{l\_\text{step5}} = \vec{b}_{\text{2nd\_ref}}. \tag{3.11}$$

And reflected signal $\vec{b}_{r\_\text{step5}}$ will be used as an input vector to calculate the next reflected signal; $\vec{a}_l$ in equation (3.3). These procedure are repeated until the reflected signal is smaller than 0.01 of the magnitude of the first reflected signal.

Each reflected signal should be converted to time signal, presented in section 2.3.1 and figure 2.9 to 2.11. Here input Gabor pulse, which is the same with that in figure 2.9 having 200-kHz center frequency, will be considered. As an example 2-mm notch depth (d_N) and 7-mm length (L_N) case was carried out. The signals of the

first, second, and third reflection are represented in figure 3.2. Figure 3.2(a) and (b) represent the first and second torsional wave mode, respectively. Each torsional mode, the first, second, and third reflected signals become smaller when more reflection is repeated. The reflected signals are summed up to represent reflection signal as shown in figure 3.3.

3.2 Numerical validation

Presented axisymmetric notch scattering in a pipe problem should be validated its compatibility. To this end numerical simulation was carried out using COMSOL multiphysics [37]. The used mode is the same with that in section 2.1.2. As notch defects notch depth (d_N) is changed from 1 to 13 mm and notch length (L_N) is changed from 1 to 20 mm with 1-mm interval, respectively. As an example, 2-mm notch depth (d_N) and 7-mm length (L_N) case is carried out and presented in figure 3.3 which result of scattering theory. Figure 3.3(a) and 3.3(b) represent reflected signal of the first and second torsional wave, respectively. Note that, simulation result went through dispersion compensation procedure. The figure 3.3 shows that the results of proposed axisymmetric notch scattering theory and numerical simulation show good agreement. To identify appearance of the reflection coefficients, L_N = 2 and 7 mm cases are presented in figure 3.4. The solid lines represent the results obtained by scattering theory and the dotted lines represent the result obtained by numerical simulation. Two figures, figure 3.4(a) and (b), show compatibility of the axisymmetric notch scattering theory and numerical simulation. Similarly to the previous results; stepped pipe scattering theory shown in figure

2.15, reflection coefficient of the first torsional wave mode shows increasing tendency and that of the second torsional wave mode increases and then decreases although there is some difference. In order to understand effect of notch length (L_N), reflection coefficients with respect to notch length are presented in figure 3.5. When notch depth is small enough, fluctuation phenomena of the reflection coefficients vary greatly. Otherwise, in case of the second torsional wave mode, when notch depth is small or large much fluctuation phenomena appears but less fluctuation is shown in medium depth of notch. It can be said that fluctuation occurs more when reflection coefficient is small. Because the reason of fluctuation occurrence is synthetic of multiple reflections, bigger change of reflection coefficient with respect to notch length (L_N) appears. Reflection coefficients with respect to notch depth (d_N) and length (L_N) for axisymmetric notch cases can be represented as reflection maps as shown in figure 3.6 which can be applied to estimate size of notch defect in a pipe.

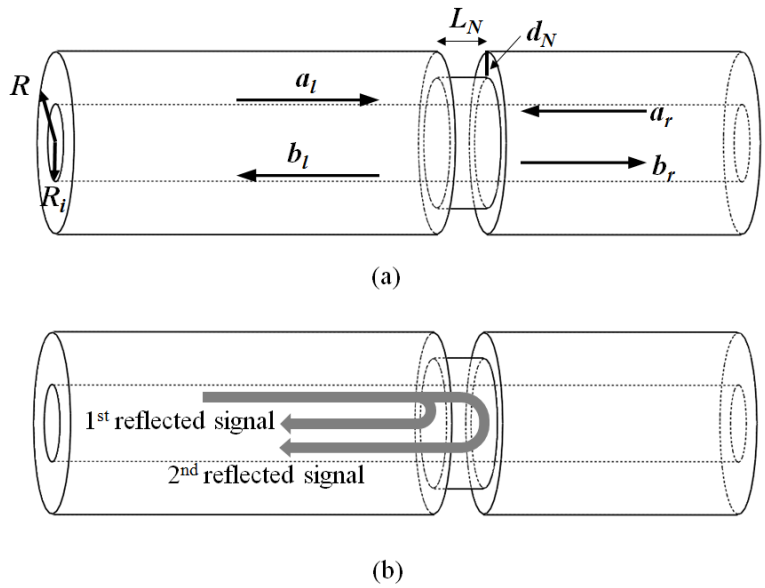

Figure 3. 1. (a) Definition of an axisymmetric notch defect problem and (b) schematics of multiple scattering at the notch defect.

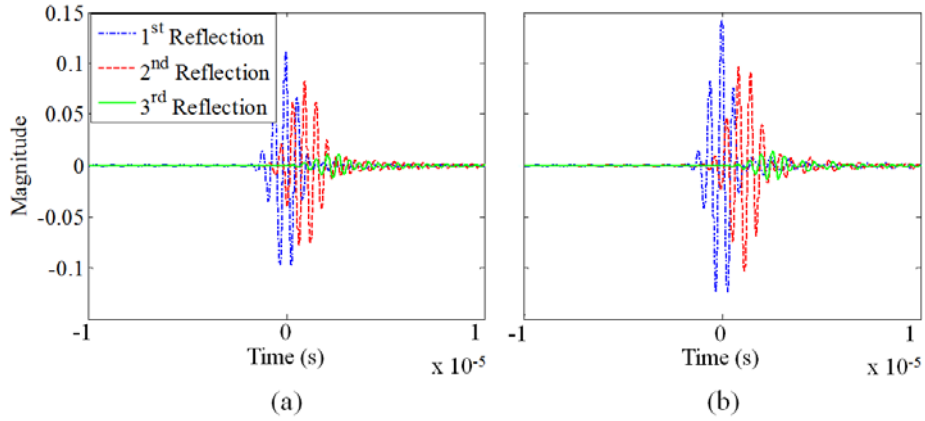

Figure 3. 2. Multiple scattering at a notch defect as shown in figure 3.1(b) for the (a) first and (b) second torsional wave modes.

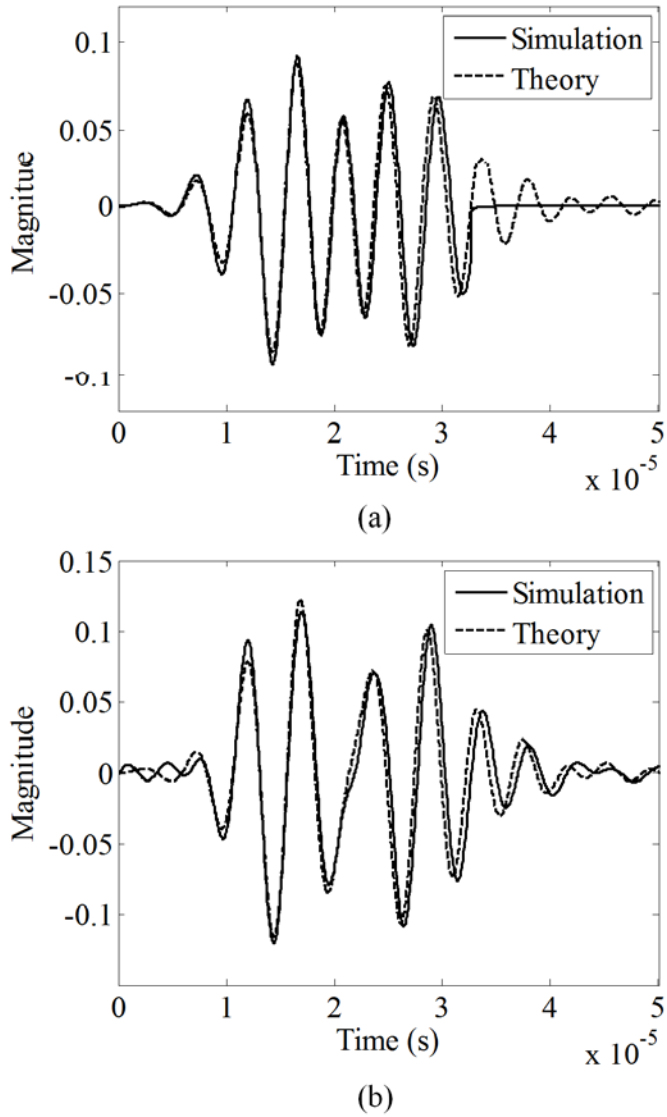

Figure 3. 3. Reflected wave of the (a) first and (b) second torsional wave modes obtained by simulation (with dispersion compensation) and notch scattering theory.

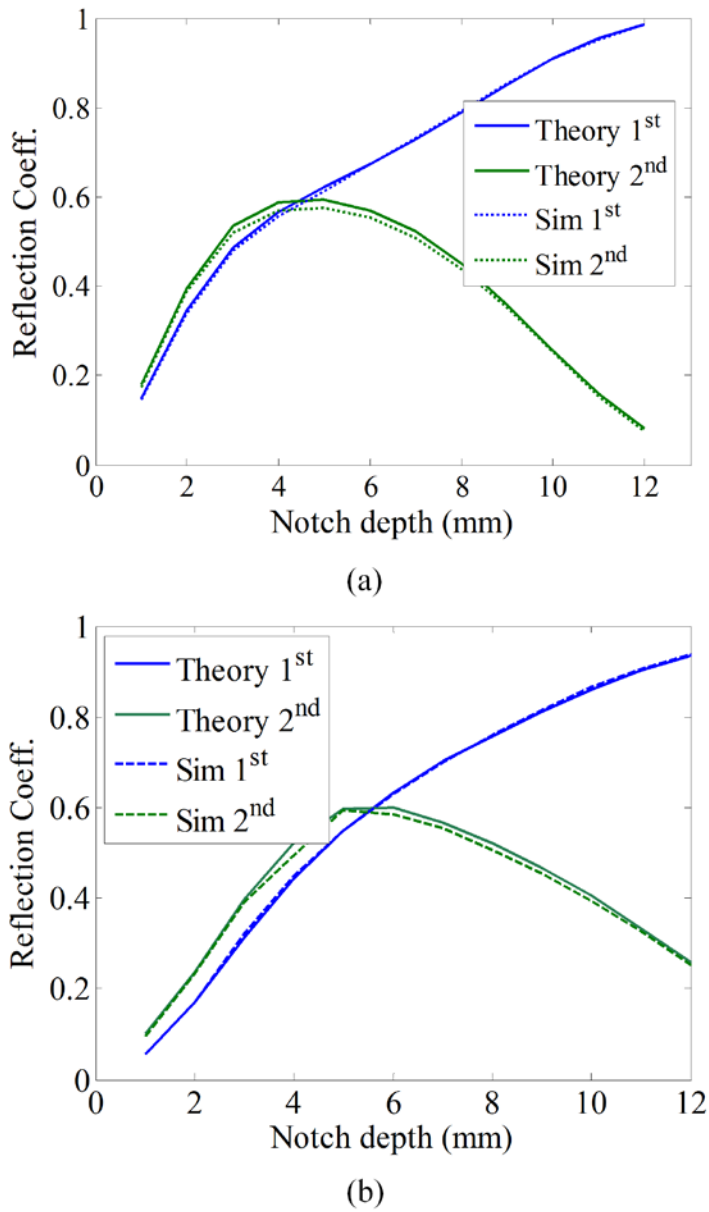

Figure 3. 4. Reflection coefficients of the first and second torsional wave mode for the axisymmetric notch length of (a) 2 mm and (b) 7 mm.

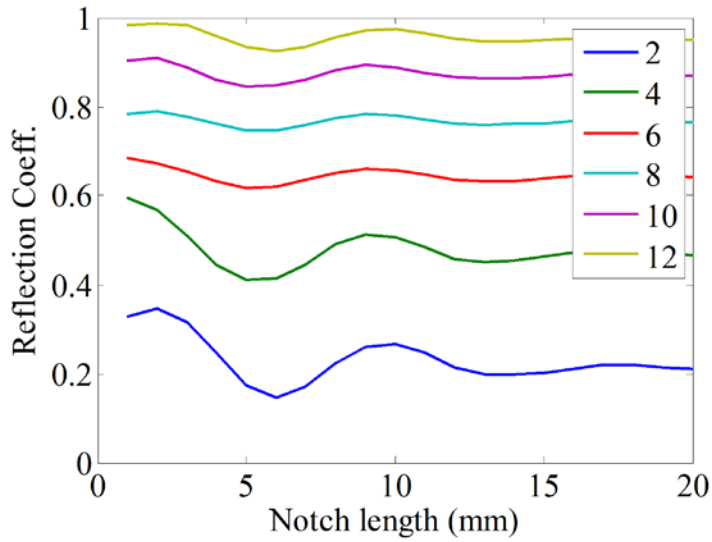

(a)

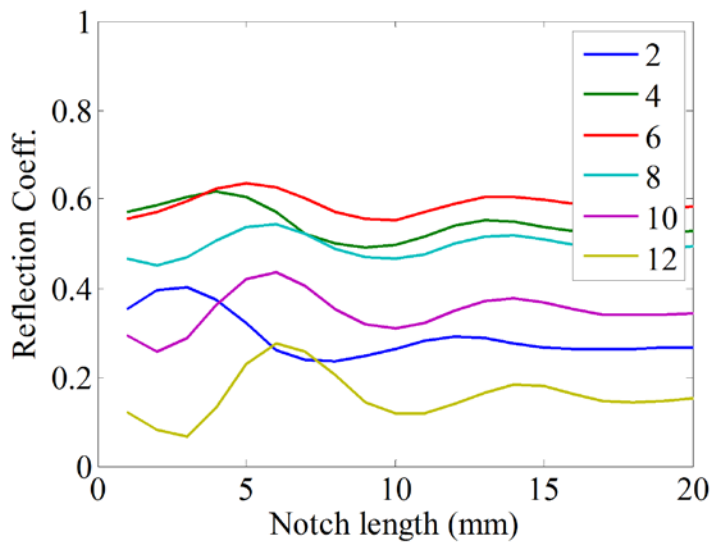

(b)

Figure 3. 5. Reflection coefficients of the (a) first and (b) second torsional wave mode for length of the axisymmetric notch. Numbers in the legend denote notch depth in mm.

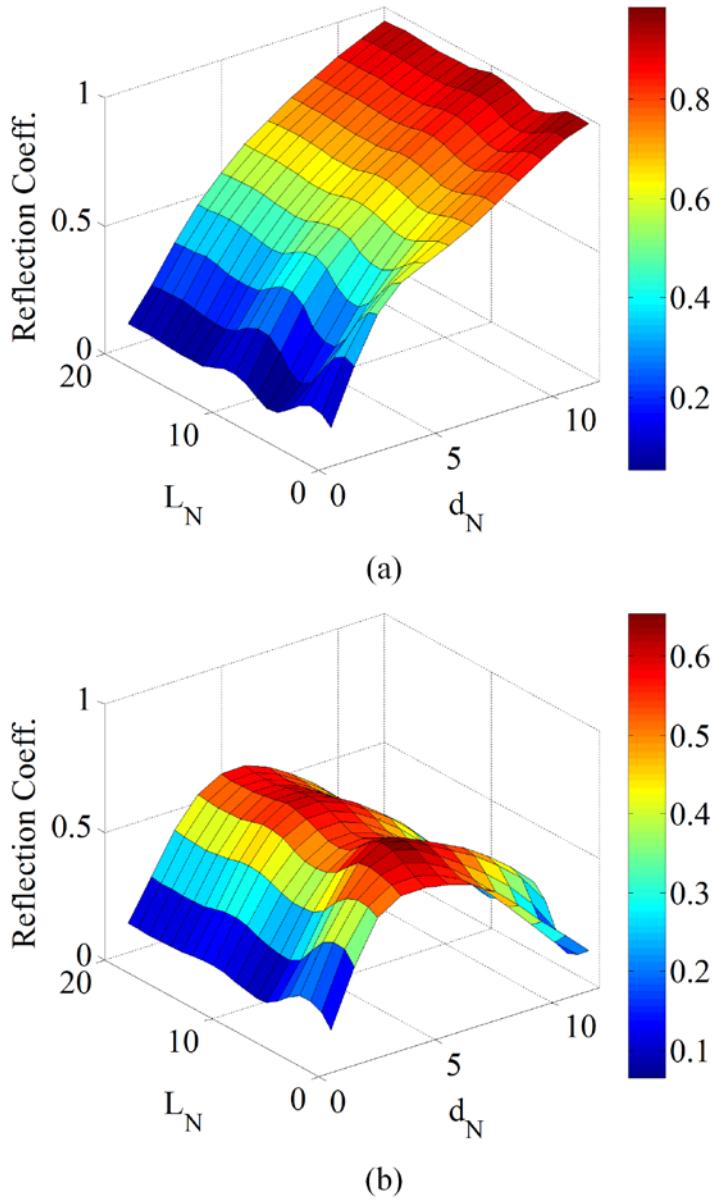

Figure 3. 6. Reflection maps of the (a) first and (b) second torsional wave modes for an axisymmetric notch having depth (d_N) and length (L_N).

CHAPTER 4.

Effect of the central angle of notch and ratio of reflection coefficients

Until now, research for scattering from an axisymmetric notch defect in a pipe was carried out. To estimate part circumferential notch, three-dimensional analyses not axisymmetric case should be considered. To this end, in this chapter, relation between the central angle of a part circumferential notch defect and reflection coefficient of each torsional mode will be demonstrated. Definition of the target notch defect is shown in figure 4.1 which are depth (d_N), length (L_N) and central angle (θ_N). First of all three dimensional transient finite element analyses for notch defects which have different central angle (θ_N) were carried out using commercial FEM tool (ABAQUS). After that, magnitude of the reflection coefficient with respect to the central angle (θ_N) will be presented. Lastly, the ratio R_{ij}, ratio of *i*-th torsional mode to the *j*-th torsional mode, will be proposed which is independent to the central angle (θ_N). This result can be used to characterize size of notch defect in the next chapter.

4.1 Finite element models

Numerical analyses based on the three-dimensional transient finite element method

were carried out by using ABAQUS [49]. Geometry of analysis model, are illustrated in figure 4.2. An aluminum pipe with 1.5-m length, 70-mm outer diameter and 13-mm thickness was considered. A notch defect is located 0.83-m away from left side. To generate only the first torsional wave mode surface traction across the pipe thickness at the left end (gray-colored in figure 4.2) was loaded as the same with the mode shape of the first torsional mode with the Gabor pulse having a center frequency of f_c = 320 kHz. Incident and reflected signals were measured by storing displacement in the circumferential direction on each node at the left edge (dotted in figure 4.2), and then all recorded signals were summed together to obtain the axisymmetric torsional modes only and eliminate flexural modes. Through this process only the axisymmetric modes; the first and second torsional modes in this case, can remain but all the flexural modes are canceled out. In analyzed pipe (13 mm) with 320 kHz frequency, the first, second and third torsional mode can exist as dotted lined in figure 2.7. Thus three modes can be expected to be reflected when the first torsoinal wave mode reflects at the notch defect. All pipe structure was constructed of hexagonal meshes having average size of 1 mm and analyzed with 0.01 μs time step. For the notch with 6-mm depth (d_N) and 10-mm length (L_N), central angle (θ_N) had been changed from 50° to 300° in addition to 360° (total 7 cases).

4.2 Numerical results

The measured signals are shown in figure 4.3. Each signal was normalized by incident signal. Thus the magnitude of each reflected mode can be treated as

reflection coefficient. T_1, T_2 and T_3 indicate the reflection coefficient of the first, second and third torsional mode, respectively. From the figure, size of signals is not changed but conservation of wave form can be confirmed. The results of reflection coefficients for notch defects which have different central angle (θ_N) but the same depth (d_N) and length (L_N) obtained by numerical analyses are represented in figure 4.4. The solid lines are virtual lines connecting origin and the results of 360° case. The dots indicate simulated reflection coefficient of each torsional mode. From the results the linearity of the reflection coefficients of each torsional wave mode to the central angle (θ_N) of notch defect is verified. It was already studied that the reflection coefficient of the first torsional wave mode is a roughly linear function of the circumferential extent of part circumferential notch defect [14, 25]. In addition, it is turned out that the second and third torsional modes have same relation in this research. The reason of proportional phenomenon of the reflection coefficients of each torsional wave mode to the central angle (θ_N) can be found in circumferential mode shapes. Two modes; the first and second torsional modes, have the same uniform circumferential mode shape which responses same aspect of reflection coefficients for the central angle of a part circumferential notch defect.

4.3 Magnitude of reflection coefficient and ratio of reflection coefficients

This time, relation between the magnitudes of each reflection coefficient and size of a notch especially central angle (θ_N) will be demonstrated. To predict it, let us define modified reflection coefficient $T_{j\_\mathrm{mod}}^{(i)}$ by multiplying $2\pi/\theta_j^{(i)}$ to the

original reflection coefficient $T_j^{(i)}$. Where, index *i* means central angle (θ_N) case (i.e., *i* = 1, 2 and 3), and *j* means torsional wave mode; 1 and 2. Thus, the modified reflection coefficient $T_{j\_\mathrm{mod}}^{(i)}$ can be written as following,

$$T_{j\_\mathrm{mod}}^{(i)} = T_j^{(i)} \times \left(2\pi / \theta_N^{(i)}\right) \tag{4.1}$$

The modified reflection coefficients $T_{j\_\mathrm{mod}}^{(i)}$ are the same with each other though different central angle cases (i.e., different *i* for the same j). From the results, it is revealed that the magnitudes of each reflection coefficient are proportional to the central angle (θ_N) of a part circumferential notch. The fact that both reflection coefficients of the first and second torsional modes are proportional to the central angle (θ_N) of part circumferential notches can provide a new variable R_{mn} which means the ratio of the reflection coefficients of the *m*-th torsional mode to the *n*-th torsional mode as following,

$$R_{mn} = T_m / T_n \tag{4.2}$$

To find more significant consequence, let us consider two different arbitrary central angle cases, $\theta_N^{(a)}$ and $\theta_N^{(b)}$. From the previous results, it is clear that each modified reflection coefficient of *j**-th mode from *i* = *a* and *i* = *b* cases is the same, i.e.,

$$T_{j^*\_\mathrm{mod}}^{(a)} = T_{j^*\_\mathrm{mod}}^{(b)}. \tag{4.3}$$

Return to the concept of R_{mn}, the ratio of the second mode to the first mode with respect to the $\theta_N^{(a)}$ case can be written as followings after applying equation (4.1)

$$R_{mn}^{(a)} = \frac{T_m^{(a)}}{T_n^{(a)}} = \frac{\left(\theta_N^{(a)} / 2\pi\right) \times T_{m\_\mathrm{mod}}^{(a)}}{\left(\theta_N^{(a)} / 2\pi\right) \times T_{n\_\mathrm{mod}}^{(a)}} = \frac{T_{m\_\mathrm{mod}}^{(a)}}{T_{n\_\mathrm{mod}}^{(a)}} \tag{4.4}$$

Equation 4.4 can be expressed as followings after applying the equality of modified reflection coefficient (equation (4.3))

$$\frac{T_{m\_\mathrm{mod}}^{(a)}}{T_{n\_\mathrm{mod}}^{(a)}} = \frac{T_{m\_\mathrm{mod}}^{(b)}}{T_{n\_\mathrm{mod}}^{(b)}} = \frac{T_m^{(b)}}{T_n^{(b)}} = R_{mn}^{(b)} \tag{4.5}$$

Consequently,

$$R_{mn}^{(a)} = R_{mn}^{(b)} = R_{mn}(d_N, L_N) \tag{4.6}$$

From the equation (4.6), it is revealed that R_{mn} is independent to the central angle (θ_N) but dependent to the depth (d_N) and length (L_N) of a part circumferential notch defect. Some results for the cases of L_N = 2 mm with the Gabor pulse having 200-kHz center frequency are represented in figure 4.5. These results clear show the ratio of reflection coefficients is independent to the central angle (θ_N) of a part circumferential notch defect. This result indicates new algorithm to characterize size of a part circumferential notch defect by considering ratios of reflection coefficients of the torsional waves from a notch defect which are independent to the central angle (θ_N).

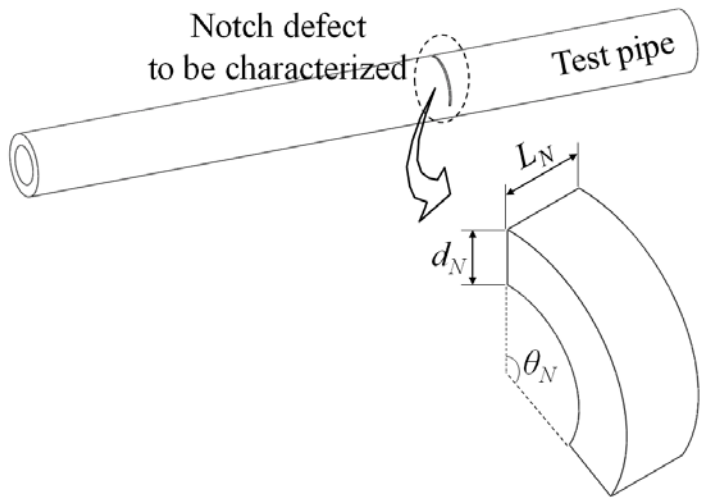

Figure 4. 1. A target part-circumferential notch defect defined as depth (d_N), length (L_N) and central angle (θ_N)

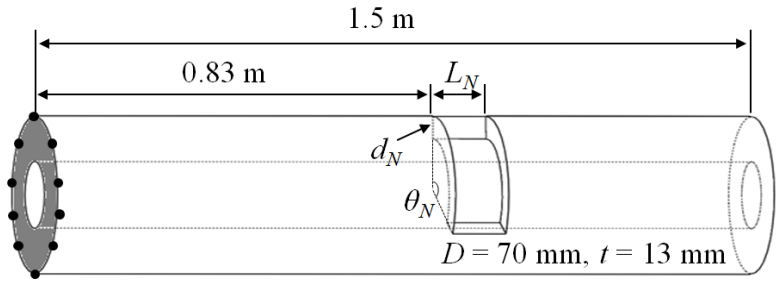

Figure 4. 2. Schematics and geometry of finite element model.

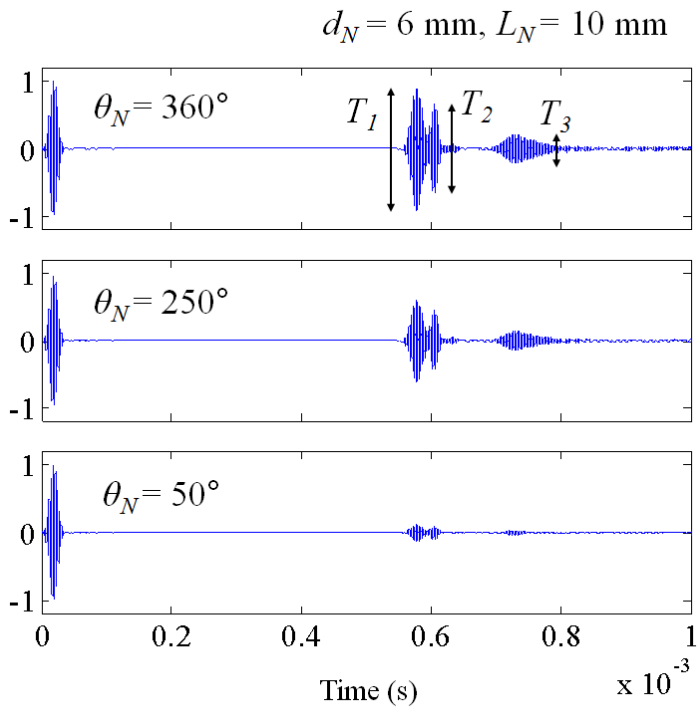

Figure 4. 3. Measured signals obtained by three dimensional finite element analysis for the model shown in figure 4.2.

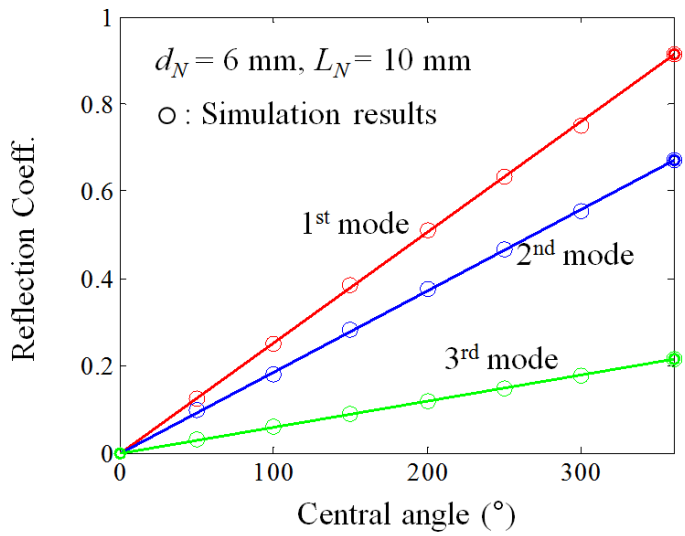

Figure 4. 4. Numerical results of reflection coefficients for notch defects varying central angle (θ_N)

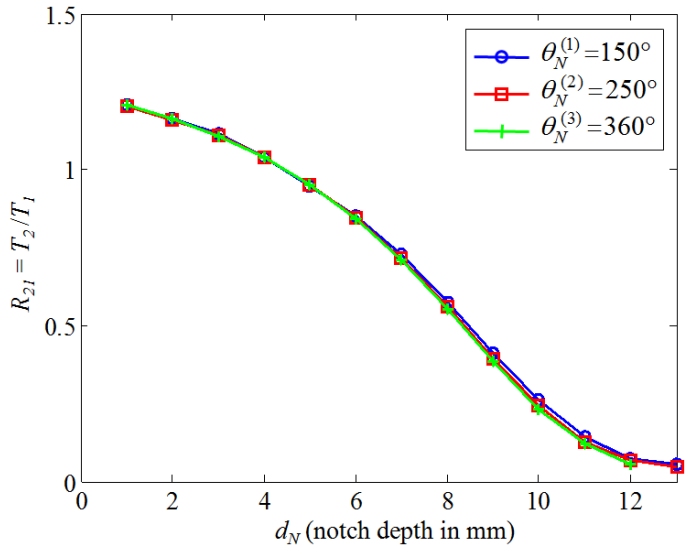

Figure 4. 5. Ratio of reflection coefficient of the 2nd torsional mode to the 1st torsional mode for the cases of L_N = 2 mm with the Gabor pulse having 200-kHz center frequency.

CHAPTER 5.

Size characterization for a notch having known length

In this chapter, a new algorithm to characterize a part circumferential notch defect having known length. This is beginning research of notch characterization which has three unknown parameter (depth, length and central angle). The reason to choose known length case for a basic research is that it has been reported to estimate length of a notch defect through frequency changes of excitation wave [23-26]. Moreover, depth of a notch defect is much important than notch length in a view of pipe safety. At first, concept of the proposed method will be represented in section 5.1. And then results of numerical analyses for axisymmetric notch with varying depth will be firstly presented in section 5.2. By using these results, characterization of notch depth (d_N) and central angle (θ_N) can be possible in section 4.3. Finally experimental validation to characterize notch depth (d_N) and central angle (θ_N) quantitatively will be presented also in section 5.3.

5.1 Concept

As shown in equation 4.6, the ratio values of the torsional modes are independent with respect to the central angle (θ_N) of a part circumferential notch defect. From this, if one tries to use the ratios of reflection coefficients to characterize size of a notch defect, it is possible to escape from complex non-axisymmetric effect of

partial central angle (θ_N). As mentioned before, notch defect characterization researches using mode conversion to the flexural wave mode have been reported. Because target notch defect has non-axisymmetric geometry, flexural wave mode should be reflected although only the first torsional wave mode is used as input wave mode. The torsional wave has uniform circumferential mode shape, otherwise flexural mode has circumferential mode shape of cos$n\theta$ for its circumferential order n. Because previous methods have used flexural modes, there is no choice to avoid complex three dimensional analyses which need lots of time and computational resources. But the proposed method uses only the axisymmetric torsional wave mode, only axisymmetric results are needed to characterize size of notch. This has a very significant advantage comparing with previous researches; need only the axisymmetric references. Now, let us begin with purpose of this chapter; notch defect size characterization for known length (L_N) case. In this section, L_N = 2 mm case will be considered. Because length of the target notch is already known, the ratio of reflection coefficients represented in equation (4.6) can be

$$R_{mn} = R_{mn}(d_N, L_N) = R_{mn}(d_N) \tag{5.1}$$

This means that the ratio of reflection coefficients is only the function of notch depth d_N. In this case, only one ratio value is needed to find out notch depth. Thus only two wave modes, the first and second torsional wave modes, are necessary to characterize remain two parameters. It can be easily inferred; to examine the two variables two conditions are necessary. Now let us suppose notch depth d_N was estimated using equation 5.1. The remain value is central angle (θ_N). This value can

be directly examined using equation 4.1. It has not been referred above, $T_{j\_\mathrm{mod}}^{(i)}$ indicates axisymmetric result of the *j*-th mode in case *i*, so that

$$T_{j\_\mathrm{mod}}^{(i)} = T_j^{(i)} \times \left(2\pi / \theta_N^{(i)}\right) = T_j^{(\theta_N = 2\pi)} \tag{5.2}$$

Thus the central angle can be calculated using

$$\theta_N^{(i)} = 2\pi \times T_j^{(i)} \Big/ T_j^{(\theta_N = 2\pi)} \tag{5.3}$$

Following two steps using equations (5.1) and (5.3), depth (d_N) and central angle (θ_N) are easily estimated with only axisymmetric reference.

5.2 Numerical analysis

To characterize depth and central angle of a notch defect having known length, two-dimensional axisymmetric reference should be prepared. To this end, finite element analyses for an aluminum pipe having 70-mm diameter and 13-mm thickness were carried out for the model represented in figure 5.1. All pipe structure was constructed of triangular meshes having average size of 1 mm and analyzed with 0.01 μs time step. In this section, known notch length case, only two torsional wave modes (the first and second modes) are needed. Thus 200-kHz of the Gabor pulse is selected as an input pulse (see dispersion curve in figure 2.7). In this situation, excitation would be very important. Because the first and second torsional modes can propagate at the excitation frequency, both two modes are excited when general transducers are used. In this research phased meander array method was employed which can make only the first torsional wave mode in a pipe

at a frequency above the first cutoff frequency [50]. More so come out in the reference, to briefly explain about the method, two meander type magnetostrictive patch transducers are located at the specific location having distance of s_T. And two transducers excite sequentially with specific time delay (t_d) for suppressing the second torsional mode and enhancing the first torsional mode. Time delay (t_d) and distance between the two transducers (s_T) can be obtained by following equations [50],

$$t_d = \lambda_2 / (c_{p2} - c_{g2}) \tag{5.4}$$

$$s_T = t_d \times c_{g2} \tag{5.5}$$

The values of time delay (t_d) and distance of the two transducers (s_T) were calculated as 13.2 μs and 32.16 mm for 200 kHz in a test pipe which has 70 mm diameter and 13 mm thickness. Where, c_{p2} and c_{g2} denote phase and group velocity of the second torsional mode which have a value of 3924 m/s and 2436 m/s. λ_1 and λ_2 denote wave length of the first and second torsional mode respectively. How this method was applied is shown in figure 5.2. Note that even though figure 5.2(a) is drawn in three-dimensionally, numerical analyses were conducted in two dimensions with axisymmetric condition. As mentioned before two transmitters, Tr. 1 and Tr. 2, are needed to excited only the first torsional wave. Each transmitter consists of two-finger meander coil, 4 individual lines, and three cycles of step function of 200 kHz frequency were loaded as concentrate force in the circumferential direction on each line. The excited functions of Tr. 1 and Tr. 2 are figured in figure 5.2(b). To find reflection coefficients, it is essential to measure magnitudes of each wave mode; incident first mode, reflected first mode and

second mode. However the second mode of the torsional wave is so dispersive that judgment of amplitude is ambiguous. Thus in this research, reflection coefficient of the first torsional wave mode (T_1) and that of the second torsional wave mode (T_2) were examined from extracted signals which has 200 kHz frequency constituent after undergoing short-time Fourier transform (STFT). Figure 5.3 shows an example signal of a part circumferential notch simulation which has thickness of 5 mm. This signal was converted from original time magnitude signals through selecting 200 kHz frequency constituent after STFT. Reflection coefficient of the first and second torsional mode can be calculated by C_1 (magnitude of the incident first torsional mode) dividing into T_1 (reflected first torsional mode) and T_2 (reflected second torsional mode) represented in figure 5.3.

Numerical simulation was conducted for depth of a notch defect (d_N) changed from 1 mm to 13 mm with 1 mm interval. After numerical simulation for the model mentioned before, the results are shown in figure 5.4. Reflection coefficients of the first torsional mode increase monotonically. In contrast, reflection coefficients of the second torsional mode show a tendency of increasing until near 5 mm depth and then decreasing. The results can be explained from the mode shapes of two torsional wave modes shown in figure 2.16 as mentioned before. In the previous researches [14, 23-25, 27], one can see very similar results with this. Note that they measured flexural modes instead of the second torsional mode and used circumferential extent as a variable. Comparing the two studies, the mode shapes of the first torsional mode in both circumferential and thickness direction have uniform sign but flexural mode and the second torsional mode have changes in sign. Similarity of the sign change of the mode shapes makes comparable trend of the

reflection coefficients. Detailed differences of the shapes induce the differences between the actual reflection coefficients.

5.3 Application

5.3.1 Experimental validation

To validate finite element studies, experiments are also needed to be carried out. Schematics of experimental setup are shown in figure 5.5. Exact location of transmitter 1, 2, receiver and notch are the same in figure 5.1. To generate and measure torsional wave modes, magnetostrictive (MS) [51, 52] patch type transducers are employed. Each transmitters and a receiver consists of MS patches, permanent magnets and meander coils. For the transmitters, meander coil is so arranged as half wavelength of the first torsional mode to enhance the first torsional mode [53-56]. Unlike transmitters, only one line of coil is applied on a receiver in order to avoid overlapping effects of wavelength. To excite individual transmitters with a specific time delay (t_d), Field-programmable gate array (FPGA) modules (Cyclone, Altera Corp., Sna Jose, CA) were employed as a two-channel function generator and multi-channel power-amplifier which had been developed using several AD797 (Analog Device) was also employed. As experimental specimens, part circumferential notches for θ_N = 250°, L_N = 2 mm and d_N = 1, 3, 5, 7 and 9 mm (i.e., 5 cases) were designed. To compare with experimental result, three-dimensional FEM simulation was carried out. The numerical model and geometry are the same in figure 5.1 and 5.3. Hexagonal meshes with average size

of 1 mm and 0.05-μs time interval are used for numerical analyses. The experimental results and simulation results are represented in figure 5.6. The reflection coefficients of the first torsional mode and second mode obtained by experiments are marked as triangle and square marker, respectively. The simulations results are represented by solid line and dashed line which indicate reflection coefficient of the first and second torsional wave modes, respectively. Even though these results are obtained for non-axisymmetric notch defect, θ_N = 250°, the results shown in the figure 5.6 have the same tendency that in the figure 5.4. As mentioned in Chapter 3, this phenomenon is due to effect of a central angle; reflection coefficient has linear relation with respect to the central angle of the notch defect. From the fact that reflection coefficients obtained by experiments and numerical analyses are in good agreement, the validity of the results are confirmed experimentally.

5.3.2 Notch estimation algorithm

If trying to infer from what we have studied so far, one can find some algorithm which can estimate depth and central angle of part circumferential notch which has specific axial extent (2 mm in this work). From now on, let us explain two-step algorithm to estimate depth and central angle of part circumferential notch defect. The algorithm consists of two steps;

Step 1: Estimate depth using the ratio of reflection coefficients,

Step 2: Estimate central angle from the magnitudes of each mode.

Before applying this algorithm, experimental results should be obtained. In this section, for the example, numerical results in Fig. 5.8 will be used which have T_1 =

0.1987, T_2 = 0.1414, Ratio =0.7145 and treated as experimental results.

Before describing in details about the algorithm, we will discuss how to get a reference for estimation of a notch defect. To diagnose size of a defect requires references and it is very important issue how to get this. In this research, to predict depth of the notch defect, the ratio of the reflection coefficients (T_2/T_1) which is the same regardless of the central angle is needed. Therefore it is possible to make a desired performance with only the result of 360° case. Also the central angle can be estimated by comparing with the result of 360° case. Note that two variables of a part circumferential notch; depth (d_N) and central angle (θ_N), can be estimated by using only the result of axisymmetric case. In this 360° case, the defect is axisymmetric, it is possible to simplify the analysis to two dimensional not three dimensional requiring a lot of calculation time.

Now, let us go back to the algorithm. The algorithm is represented in figure 5.7. A line in figure 5.7(a) and two lines in figure 5.7(b) are the results of 360° case. figure 5.7(a) represents Step 1; estimate depth using the ratio of reflection coefficients. As mentioned before, ratio of the reflected second mode to the first mode is the same despite different central angles. By comparing value of ratio obtained by experiment with 360° reference, depth of a part circumferential notch can be estimated. Going back to the example, the value of the ratio of reflection coefficients is 0.7145, consequently the depth of the notch can be estimated as 6 mm as following arrows in figure 5.7(a).

The second step is represented in figure 5.7(b). Obtained reflection coefficients from the example are marked, T_1 = 0.1987 and T_2 = 0.1414, in the figure. Central angle can be calculated by finding θ_N to match the value with one of 360° result

using the equation (5.3). Reflection coefficients of the first and second torsional mode in 360° case of 6 mm thickness are 0.3498 and 0.2932, respectively. Because we have two reflection coefficients; those of the first and second modes, equation (3) can be used twice. Estimated depth and ratio of two modes was adjusted in step 1, however, two equations from the first and second mode give unique value of θ. In this example, θ = 250° is calculated. The example is the result of FE method so that estimated depth and central angle have exactly the same value.

In order to validate the proposed algorithm, experiments for several part circumferential notch defects whose depth and central angle are listed in table 5.1 were carried out. These notch defects also have 2 mm axial extent. Note that the four defects have same cross section area difficult to be distinguished from each other. The obtained experimental results; reflection coefficients of the first and second torsional modes and those ratio (T_2/T_1), are also provided in table 1. From these results depth and central angle of part circumferential notch can be estimated by following two-step algorithm explained before.

Estimated depth (d_N), central angle (θ_N) and errors are listed in table 5.1. Mean error was calculated as 4.34 % and maximum error did not exceed 8 %. From the result, it is shown that proposed two-step algorithm works to estimate a part circumferential notch defect having known axial extant.

Case	Estimation of d_N		Estimation of θ_N	
	Given	Estimated [error]	Given	Estimated [error]
Case 1	4.04 mm	4.35 mm [7.7 %]	360°	343° [4.6 %]
Case 2	6.00 mm	6.38 mm [6.3 %]	250°	247° [1.2 %]
Case 3	7.29 mm	6.84 mm [6.2 %]	210°	219° [4.3 %]

Table 5. 1. Size of the part circumferential notch defects of real and estimated experimentally.

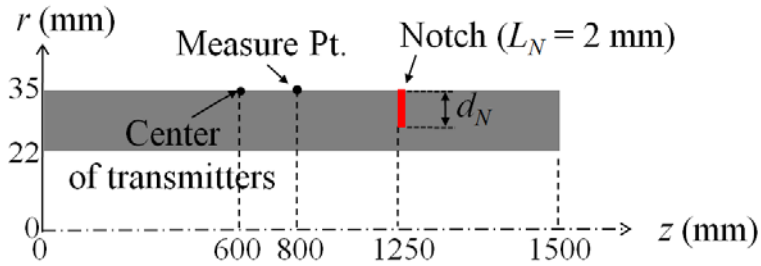

Figure 5. 1. Schematics and geometry of FEM model for two-dimensional analysis.

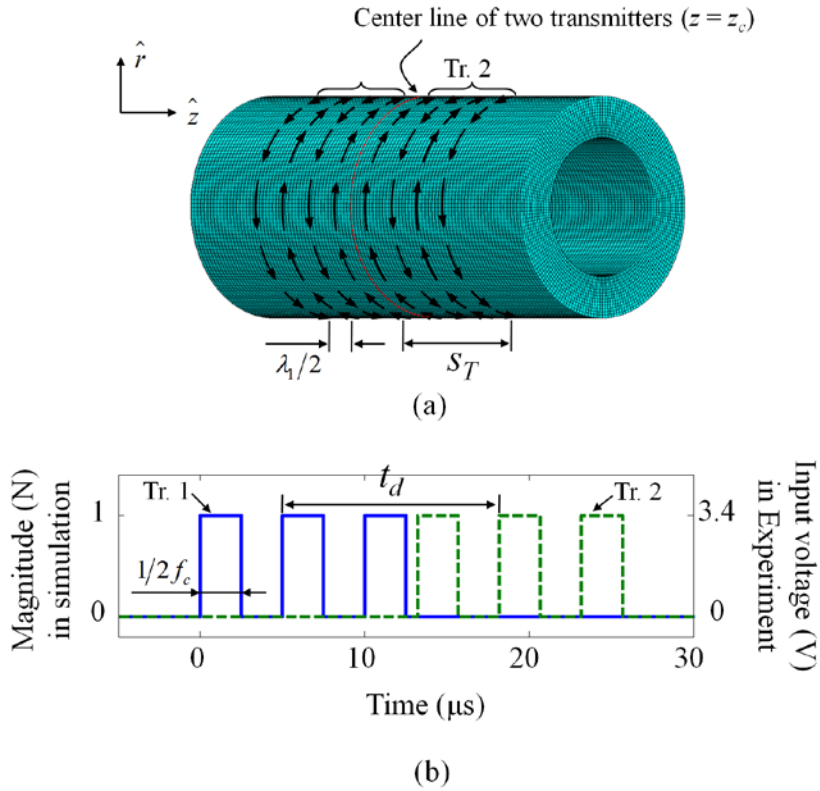

Figure 5. 2. (a) Schematics of transmitter system, phased meander array method. For exciting frequency of f_c = 200 kHz in a test pipe, wave length (λ_1) is 15.7 mm and distance between two transducers (s_T) is 32.16 mm. (b) Input signals of transmitter system. See figure 4.2 for geometry of the test pipe and location of transmitter, receiver and notch.

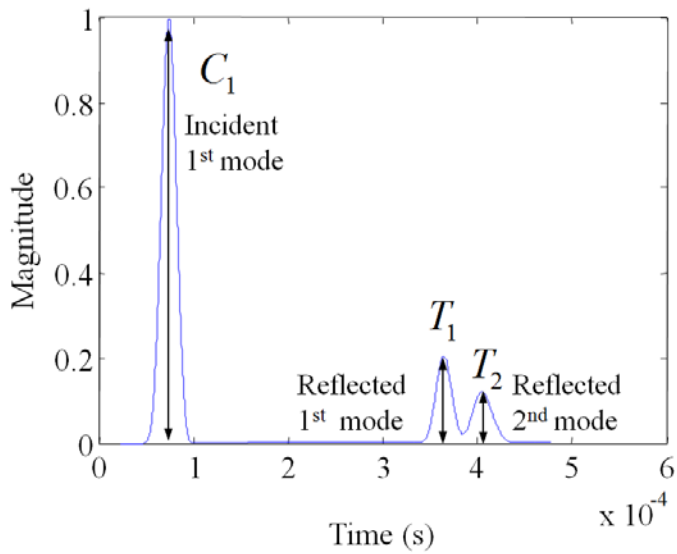

Figure 5. 3. Measured signals of numerical analysis for d_N = 5 mm notch which was transformed by short-time Fourier transform and selected 200 kHz frequency constituent.

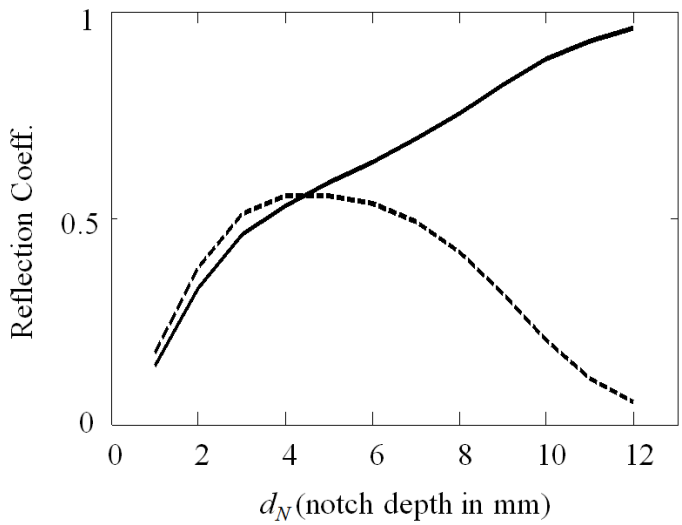

Figure 5. 4. Reflection coefficients obtained through STFT for a incident Gabor pulse with 200-kHz center frequency.

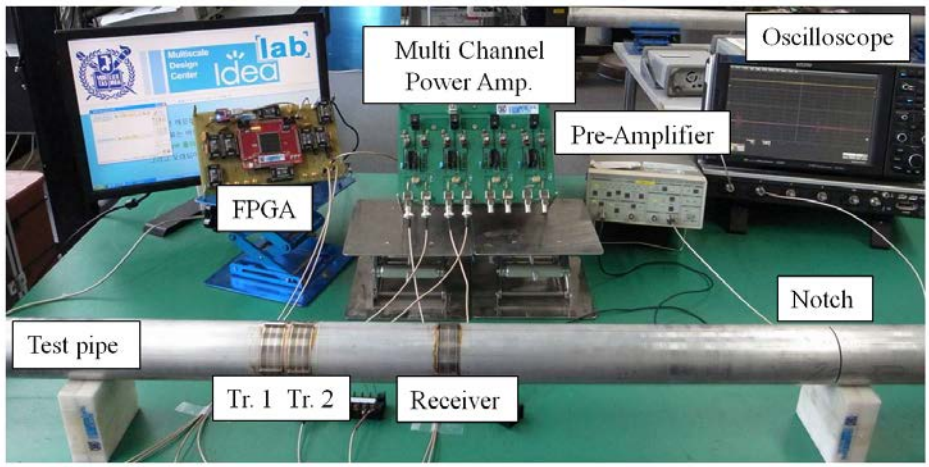

Figure 5. 5. Experimental setup. See the figure 5.1 and 5.2 for exact location of transmitter 1, 2, receiver and notch.

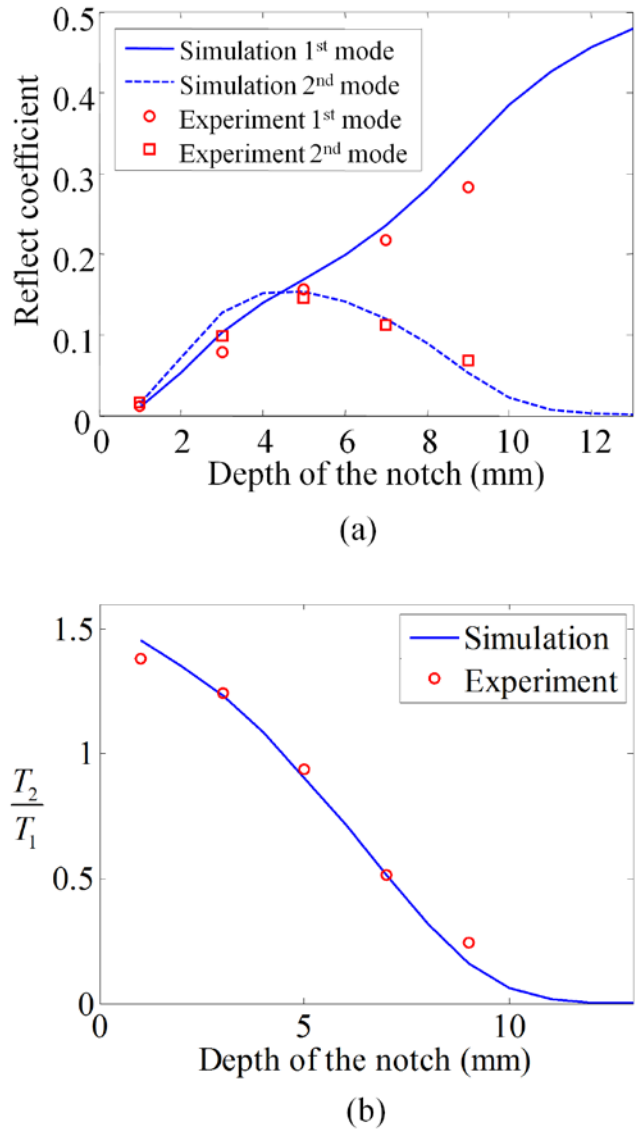

Figure 5. 6. (a) Simulation and experiment results of 250° notch case and (b) ratio of the second torsional mode to the first torsional mode.

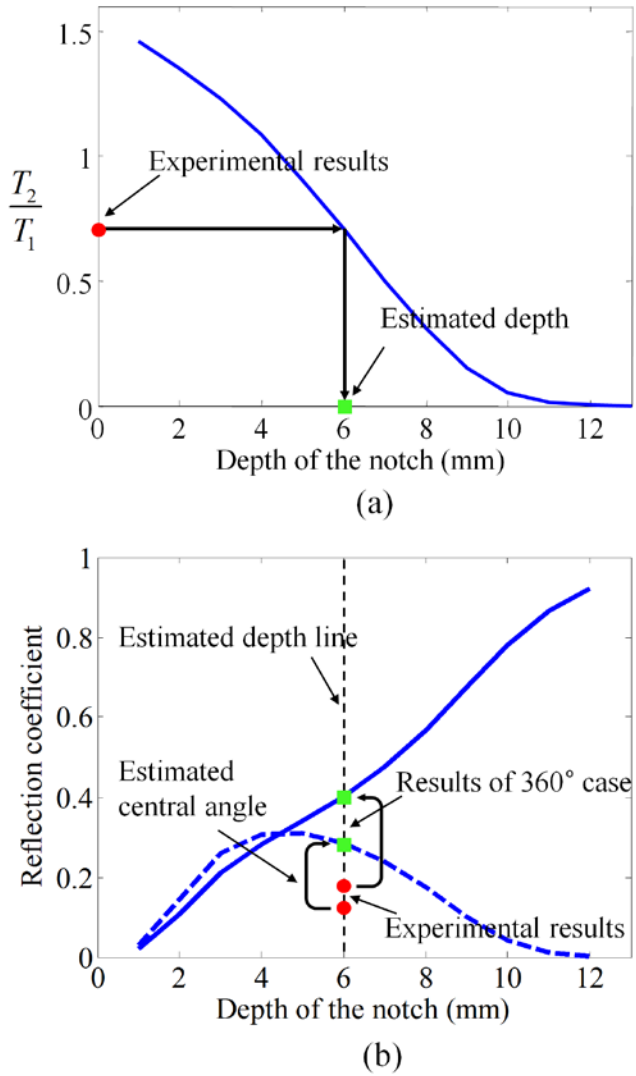

Figure 5. 7. Schematics of two-step algorithm for estimating depth and central angle of a part circumferential notch. (a) Step 1 and (b) step 2.

CHAPTER 6.

Part circumferential notch characterization

In this chapter, the algorithm to characterize a part circumferential notch defect having known length in previous chapter will be expanded for a part circumferential notch defect which has three unknown parameters (depth d_N, length L_N and central angle θ_N) to be characterized. In section 6.1 reflected coefficients which were calculated in CHAPTER 3 and expanded in three-dimensionally in CHAPTER 4 will be validated experimentally. And then an algorithm to characterize size of notch defect will be proposed in section 6.2. The proposed algorithm will be validated experimentally by real crack estimation in section 6.3. These procedures will be discussed in section 6.4

6.1 Experimental validation of scattering theory for a part circumferential notch defect

An axisymmetric notch scattering theory was carried out in CHAPTER 3. This theory is for axisymmetric notch which is not a part circumferential notch defect which is to be characterized in this research. Through CHAPTER 4 linearity of reflection coefficients of each torsional wave mode with respect to central angle (θ_N) was confirmed. Combining these two phenomenons scattering of a part

circumferential notch defect can be obtained. In this section this scattering theory for a notch defect will be demonstrate experimentally.

6.1.1 Experimental setup

Experiments were conducted with the environments as shown in figure 5.5. Almost all environments were the same with those in section 5.3 but transducer configuration was different represented in figure 6.1. Because experiments would be conducted with 333-kHz Gabor pulse, many torsional wave modes can exist until the third torsional wave mode. Thus, the method to send the first torsional wave only at a frequency higher than the second cut-off frequency at which the second and third torsional modes can propagate in addition to the first torsional wave mode should be employed. The employed method is similar to the way presented in section 5.2 and 5.3, phased meander array method [50]. But in contrast to the previous method, this time two torsional modes; the second and third modes, should be suppressed. Thus 4-channel transducers should be employed. Figure 6.1 represents a 4-channel transducer array. Two transducers in each set, for example Tr. 1 and Tr. 2 in Set 1, suppress the third torsional wave mode; each set generates signals consist of the first and second torsional wave modes with the conditions as followings

$$s_{13} = \lambda_3 \big/ \left(c_{g3} - c_{p3} \right) = 12.02 \text{ mm} \tag{6.1}$$

$$t_{13} = s_{13} \times c_{g3} = 5.626 \text{ μs} \tag{6.2}$$

where, s_{13} and t_{13} denote distance of transducers in each Set and their time delay, respectively. λ_3, c_{g3} and c_{p3} are wave length, group velocity (2137 m/s), and phase velocity (4583 m/s) of the third torsional wave mode. And two sets which generate the first and second torsional wave modes (the third mode was suppressed) suppress the second wave mode with the conditions;

$$s_{12} = \lambda_2 \Big/ \left(c_{g2} - c_{p2} \right) = 61.66 \text{ mm} \tag{6.3}$$

$$t_{12} = s_{12} \times c_{g2} = 21.26 \text{ μs} \tag{6.4}$$

where, s_{12} and t_{12} denote distance of Sets and their time delay, respectively. λ_2, c_{g2} and c_{p2} are wave length, group velocity (2900 m/s), and phase velocity (3377 m/s) of the third torsional wave mode. After these procedures, only the first torsional wave mode propagates at a frequency higher than the second cut-off frequency. Each transducer is controlled by Field-programmable gate array (FPGA) modules (Cyclone, Altera Corp., Sna Jose, CA) which can enter time delay and magnitude for each transducer by the developed LABVIEW program. The configuration of the employed transducers, magnetostrictive patch type transducer, is the same is that explained in section 5.3.1. The measured signals underwent signal process; dispersion compensation which was explained in 2.3.2.

6.1.2 Experimental Validation

At first, validation of linearity of reflection coefficients with respect to central angle (θ_N) was carried out. Notch defects which have 6-mm notch depth (d_N) and 6-

mm notch length (L_N) in common, and three central angle (θ_N) were conducted. As simulation results (represented by lines in figure 6.2), lines connecting from axisymmetric notch scattering theory to the origin were used. The experimental results are shown in figure 6.2. From the figure, linearity of the reflection coefficient of the torsional wave modes experimentally confirmed. For verification about effect of the notch depth (d_N), notch defects which have 6-mm length (L_N) and 200° central angle (θ_N) in common and three cases of notch depth (d_N); 3, 6 and 9 mm, were conducted. Because we analyzed only the axisymmetric notch scattering theory, to obtain part circumferential notch defect scattering the result should be changed from axisymmetric theory using linearity for central angle. Simulation results in figure 6.3 obtained by multiplying the results of axisymmetric theory by $\theta_N/360^\circ = 200^\circ/360^\circ$. The experimental results are represented in figure 6.3 which show good agreement with scattering theory. Finally, effect of notch length was confirmed. To this end, experiments for three notch defects having 6-mm depth (d_N) and 200° central angle (θ_N) in common and three defect length (L_N); 2, 6 and 10 mm were conducted. The same way in previous experiments, simulation results are multiplied by $\theta_N/360^\circ = 200^\circ/360^\circ$ to obtain part circumferential results. Both experimental and simulation results are shown in figure 6.4. The results are seemed to be good agreement between the experimental results and simulation results. But influence of the notch length is small, the results are not meaningful greatly.

6.2 Algorithm to estimate notch defect

6.2.1. Estimation of the notch length for axisymmetric case

In chapter 5.3, notch size characterization algorithm for known length case was carried out. Here, notch depth (d_N) and length (L_N) characterization will be proposed first. And then central angle (θ_N) can be easily estimated using linearity of reflection coefficients with respect to the central angle (θ_N). In figure 3.6 in chapter 3.2, reflection maps were plotted for the first and second torsional wave mode. By using these results let us consider an example to characterize depth and length of notch defect. For the first example, $T_1 = 0.2833,\ T_2 = 0.4780$, will be considered where T_1 and T_2 are reflection coefficients of the first and second torsional wave modes respectively. The suggested two reflection coefficients were obtained by numerical simulation for an axisymmetric notch having 3-mm depth and 5-mm length. Now, one can plot contours of reflection maps which have the specific value of $T_1 = 0.2833,\ T_2 = 0.4780$ and these are represented in figure 6.5. Colors of two lines denote the value of reflection coefficients for each wave mode shown in a legend. From the figure, it is a matter of course that one can estimate the intersection as a candidate of defect geometry $d_N^*,\ L_N^*$ which are estimated depth and length respectively. These values are $d_N^* = 3$ mm and $L_N^* = 5$ mm, which are exactly the same with real notch size. Because these results are induced form numerical result which shows almost perfect agreement with reference scattering theory, size of notch is perfectly characterized. Let us consider the other example for an axisymmetric notch having 3-mm depth and length and the reflection

coefficients are $T_1 = 0.4868$, $T_2 = 0.5353$. Contours for these values are shown in figure 6.6. In contrast with previous example, this case has three different candidates; $(L_N, d_N) = (3,3)$, $(7,4)$ and $(13,4)$. To find an appropriate point among three candidates, shape of candidates is investigated shown in figure 6.7. Note that these signals were obtained from scattering theory for $(L_N, d_N) = (3,3)$, $(7,4)$ and $(13,4)$. By comparing these signals and measured signal, an appropriate candidate can be chosen. The measured signal and that of candidates for the first and second torsional wave modes are shown in figure 6.8 and 6.9, respectively. Measured signals are processed by dispersion compensation presented in section 2.3.2. The signals of the candidate 1 are the most similar to those of the measured signals. Thus candidate 1 is appropriate, which is the same with real size of notch defect.

6.2.2. Notch size characterization using reflection ratio map

In this section, notch characterization method for a part circumferential notch defect which has three geometric parameters to be inspected; depth d_N, length L_N and central angle θ_N. The characterization algorithm can be accomplished by putting together previous estimation method for a notch having known length and for a notch length in an axisymmetric case in section 5.3 and section 6.2.1, respectively. In previous section, to estimate depth and length of an axisymmetric notch defect, reflection coefficient maps were used. In contrast with previous method, in this case, depth and length of a part circumferential notch defect (not

axisymmetric) should be estimated. Thus ratios of reflection coefficients for each torsional wave modes should be calculated similar with proposed characterization method in section 5.3 known length case. The ratios R_{12} and R_{23} are

$$R_{12} = T_1 / T_2 \,, \tag{6.5}$$

$$R_{23} = T_2 / T_3 \,, \tag{6.6}$$

where, T_1, T_2 and T_3 indicate reflection coefficient of the first, second and third torsional wave mode, respectively. R_{12} and R_{23} are represented in figure 6.10. With this two ratio maps one can estimate depth and length of part circumferential notch in a similar method in section 6.2.1. And then central angle of a notch defect can be estimated by comparing reference results obtained axisymmetric scattering theory using equation (5.3).

6.3 Part circumferential notch estimation

As an example experimental result for a part circumferential notch which has 9-mm depth, 6-mm length and 200° central angle. The experiments were carried out in the aforementioned environment in section 6.1.1. Note that excitation frequency is 333 kHz at which the first, second and third modes can exist. The measured signal is shown in figure 6.11. As mentioned before, two dispersive modes; the second and third modes, should be compensated its dispersion. In figure 6.11 compensated signals after applying dispersion compensation method explained in section 2.3.2 are also represented. After going through such processes, reflection coefficients of each torsional wave mode can be obtained as

$T_1 = 0.46,\ T_2 = 0.182$ and $T_3 = 0.144$. From these values the ratios can be calculated as $R_{12} = 2.527$ and $R_{23} = 1.264$. Contours which have $R_{12} = 2.527$ and $R_{23} = 1.264$ represented in figure 6.12. From the figure candidate d_N^* and L_N^* can be decided as d_N^*=8.95 mm $L_N^* = 6$ mm . Now, to estimate central angle $\left(\theta_N^*\right)$ of defect, reflection coefficient of the first torsional wave mode obtained by axisymmetric scattering theory for d_N=8.95 mm $L_N = 6$ mm will be used which has a value of $T_1^{(\theta_N = 2\pi)} = 0.6372$. From the equation (5.3) which is $\theta_N^{(i)} = 2\pi \times T_j^{(i)} \Big/ T_j^{(\theta_N = 2\pi)}$, estimated central angle $\left(\theta_N^*\right)$ can be calculated as $\theta_N^* = 2\pi \times 0.46/0.6372 = 198^\circ$. This estimated size $\left(d_N^*, L_N^*, \theta_N^*\right) = (8.95, 6, 198)$ shows that it is very similar to real defect size $\left(d_N, L_N, \theta_N\right)_{\text{real}} = (9, 6, 200)$. Two experimental defect estimation results, including example before, are shown in table 6.1. The results show maximum deviation of 1 mm, 0.9 mm and 14° for notch depth, length and central angel, respectively. From the results, the proposed characterization method for a part circumferential notch defect is validated its effectiveness to make an accurate estimate of defect size.

6.4 Discussion

Although defect characterization results in section 6.3 show accurate performance, this method does not guarantee a unique candidate for all defect size. To show this, another example which has 6-mm depth, 6-mm length and 200° central angle was conducted experimentally. In this case measured reflection coefficients of each torsional wave modes are $T_1 = 0.3667$, $T_2 = 0.2525$ and $T_3 = 0.0778$ and ratios of reflection coefficients are obtained as $R_{12} = 1.452$ and $R_{23} = 3.246$. Contours about these ratios are represented in figure 6.13. As can be confirmed in the figure, this case has two candidates. In section 6.2.1, appropriate size could be selected among several candidates by comparing wave shape of measured signal and candidates. But comparison of signals is very hard in real experimental signal. Thus proposed characterization has limitation for uniqueness of candidate. However, the fact that length (L_N) of notch defect can be easily estimated has been researched. Just by using simple frequency sweep experiments, one can find notch length. If notch length is predicted in advance, remain depth and central angle can be estimated by using known length notch characterization method proposed in CHAPTER 5. In this way, part circumferential notches including three notch cases in section 6.3 and 6.4 were estimated with and the results are shown in table 6.2. The maximum deviation of notch depth (d_N) and central angle (θ_N) does not exceed 0.563 mm and 29°. From the results, effectiveness of the proposed notch characterization method is validated.

Case 1	d_N = 9 mm d_N* = 8.95 mm	L_N = 6 mm L_N* = 6 mm	θ_N = 200° θ_N* = 198 °
Case 2	d_N = *3* mm d_N* = *3.1* mm	L_N = 6 mm L_N* = 5.1 mm	θ_N = 200° θ_N* = 186 °

Table 6. 1. Real notch defect size and estimated notch size.

L_N (mm) given	d_N (mm)	θ_N (°)	d_N* (mm)	θ_N^* (°)	Δd_N (mm)	$\Delta\theta_N$ (°)
6	3	200	3.56	171	0.56	-29
2	6	200	6.563	194	0.563	-6
6	6	150	6.245	143	0.245	-7
6	6	200	6.359	198	0.359	-2
6	6	250	6.375	248	0.375	-2
10	6	200	6.452	191	0.452	-9
6	9	200	8.92	199	-0.08	-1

Table 6. 2. Lists of the notch characterization for given notch length. Δd_N and $\Delta\theta_N$ denote deviation of depth and central angle, respectively.

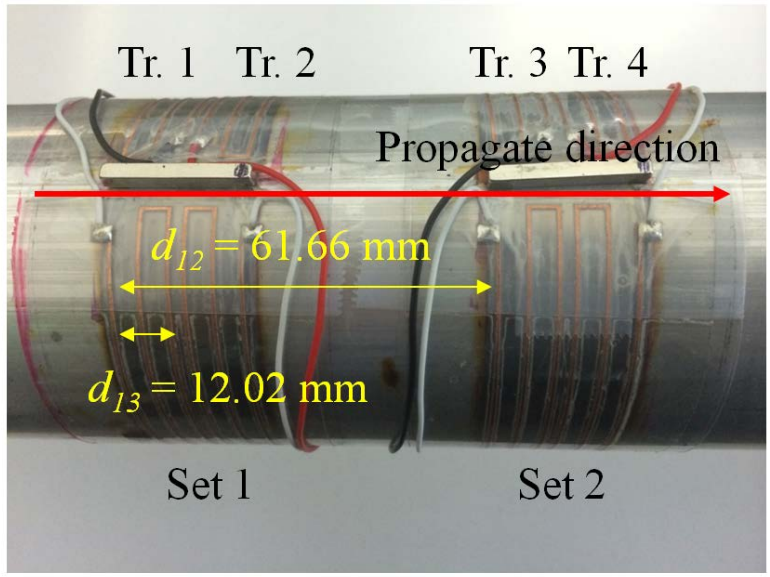

Figure 6. 1. Schematics of transducers for generating only the lowest torsional wave mode at a frequency above second cut-off frequency.

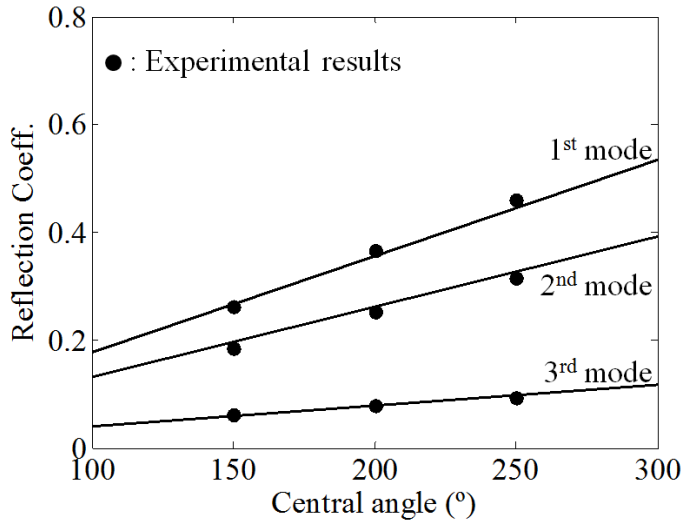

Figure 6. 2. Experimental results for central angle (θ_N) of the notch defect having 6-mm depth and 6-mm length. Lines connect from result axisymmetric notch scattering theory (360°) to the origin.

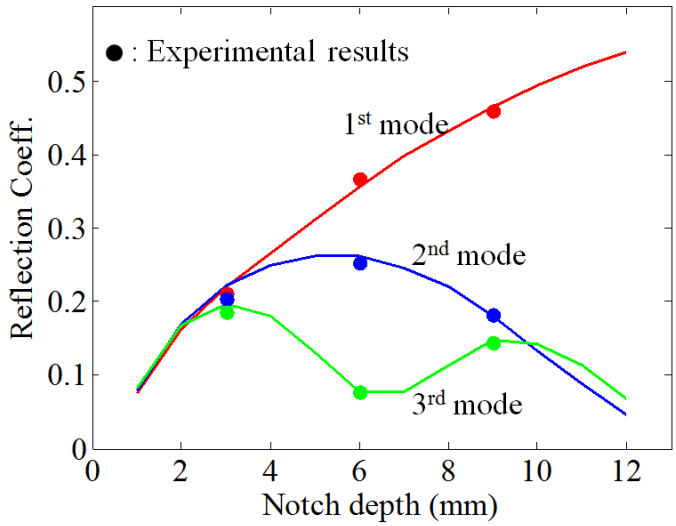

Figure 6. 3. Experimental and theoretical results for notch defects having 6-mm length and 200° central angle. Simulation results are obtained by multiplying the results of axisymmetric theory by $\theta_N/360^\circ = 200^\circ/360^\circ$.

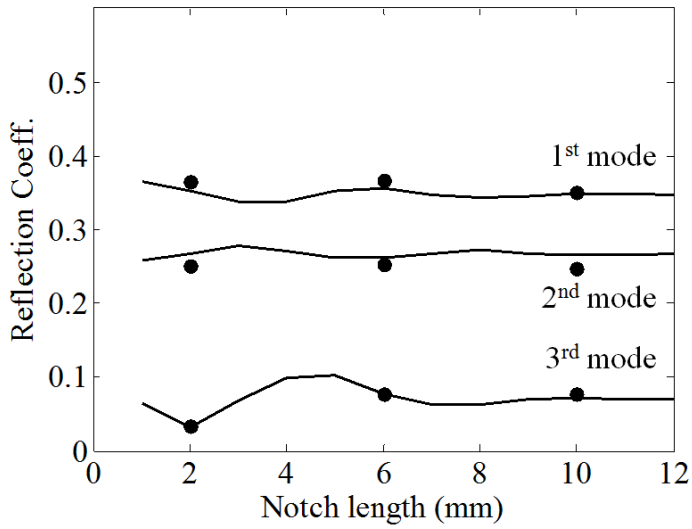

Figure 6. 4. Experimental results for notch defects having 6-mm depth and 200° central angle. Simulation results are multiplied by $\theta_N/360^\circ = 200^\circ/360^\circ$ to obtain part circumferential results

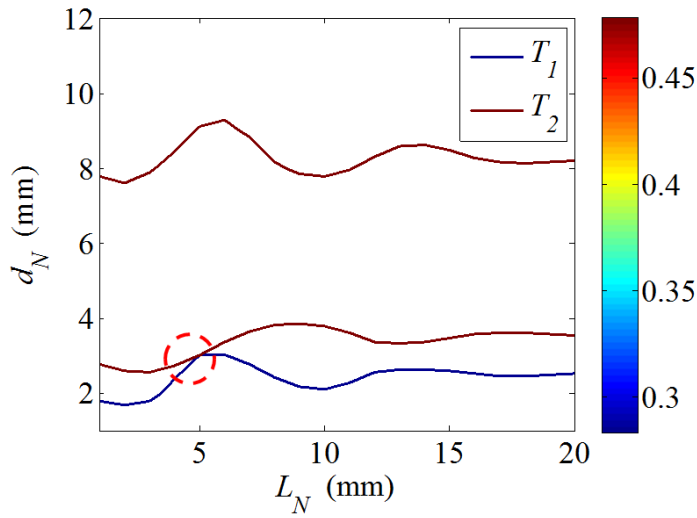

Figure 6. 5. Contour plot of reflected first and second torsional wave modes for an axisymmetric notch having 3-mm depth and 5-mm length.

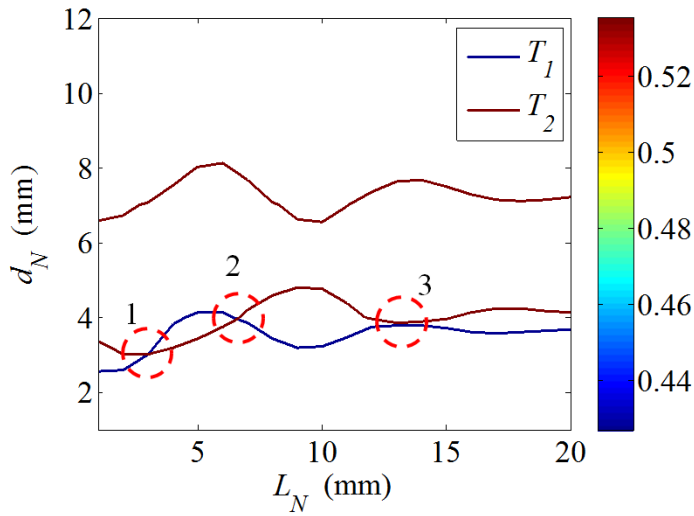

Figure 6. 6. Contour plot of reflected first and second torsional wave modes for an axisymmetric notch having 3-mm depth and 3-mm length.

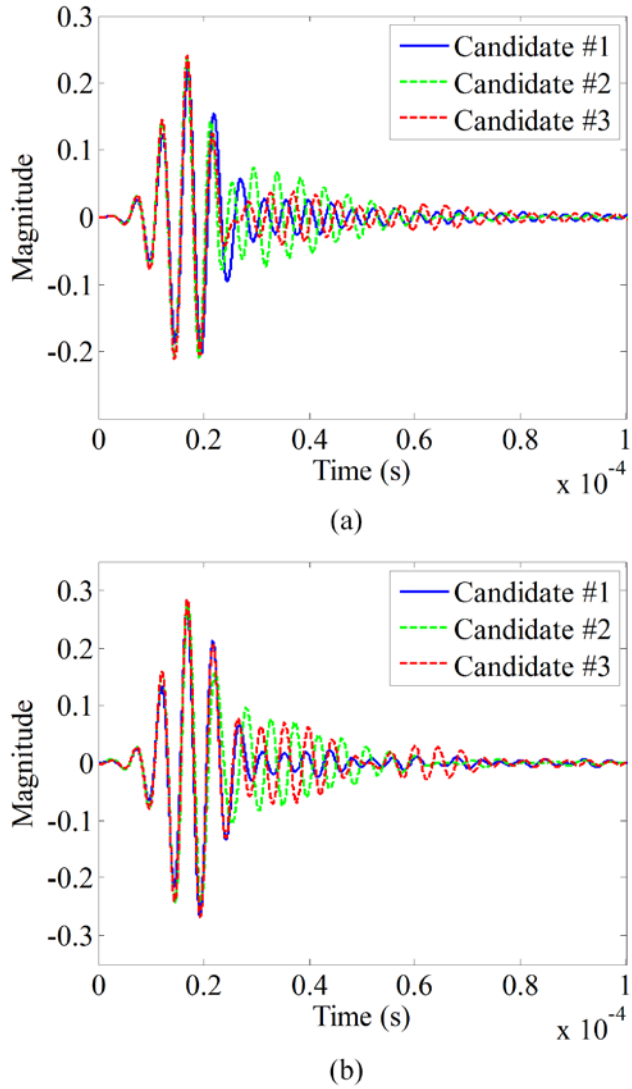

Figure 6. 7. Shapes of candidates for the (a) first and (b) second torsional wave modes. Three candidates denote $(L_N, d_N) = (3,3)$, $(7,4)$ and $(13,4)$.

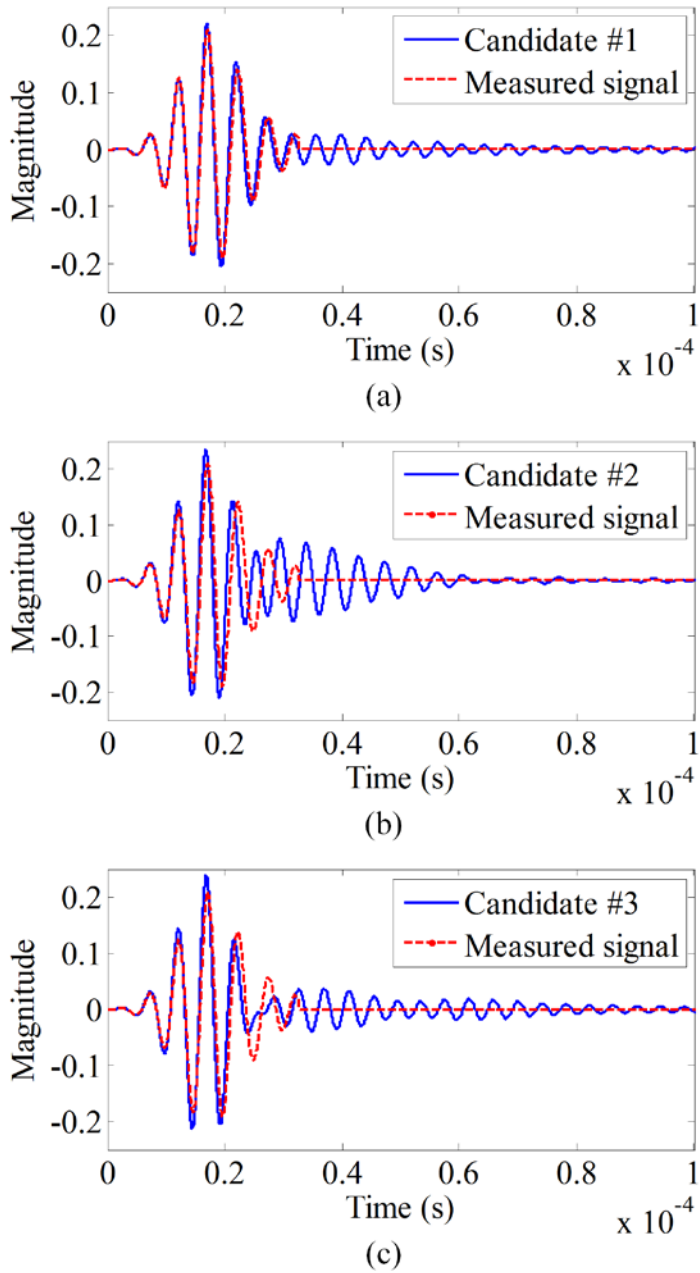

Figure 6. 8. Measured signal and that of candidates for the first torsional wave modes.

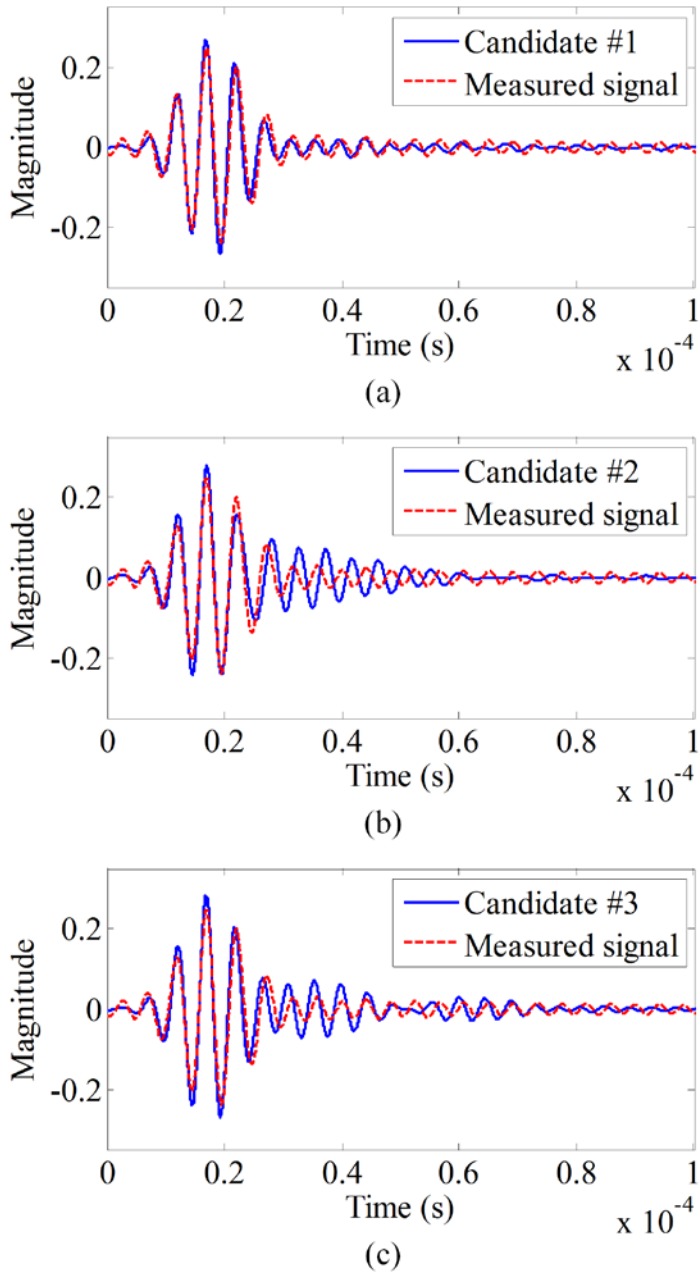

Figure 6. 9. Measured signal and that of candidates for the second torsional wave modes.

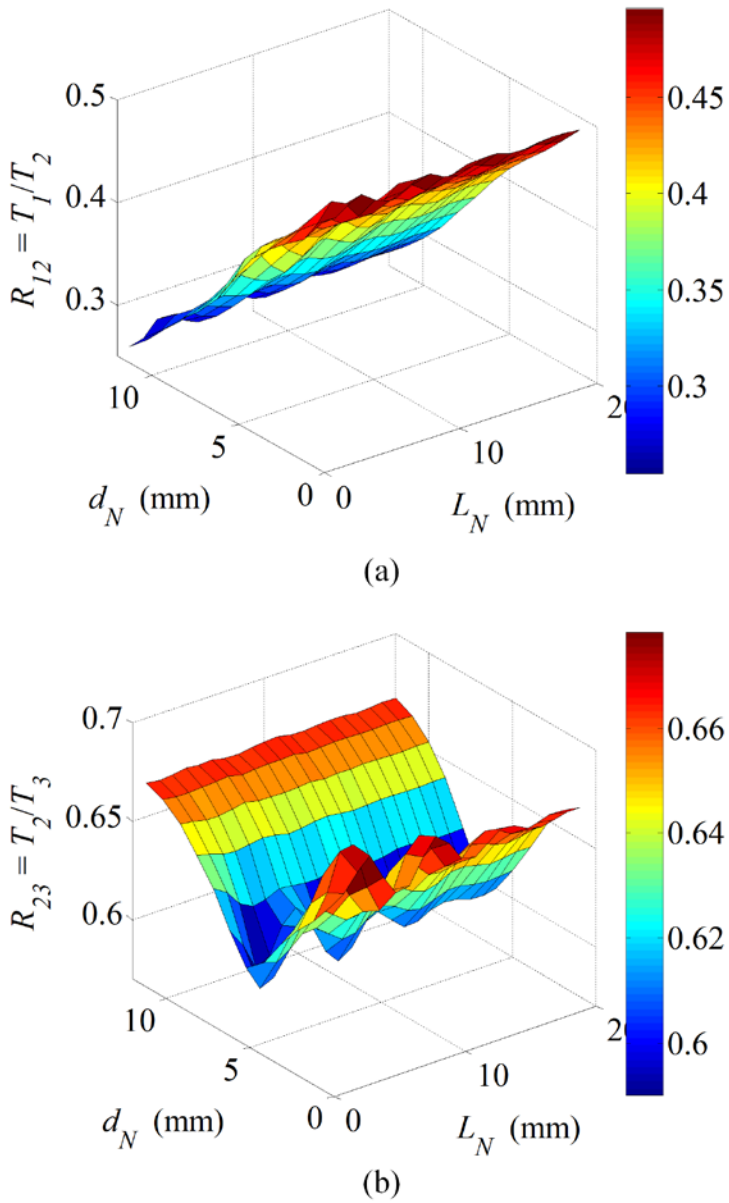

Figure 6. 10. Ratio of (a) the first torsional mode to the second one and (b) the second one to the third one.

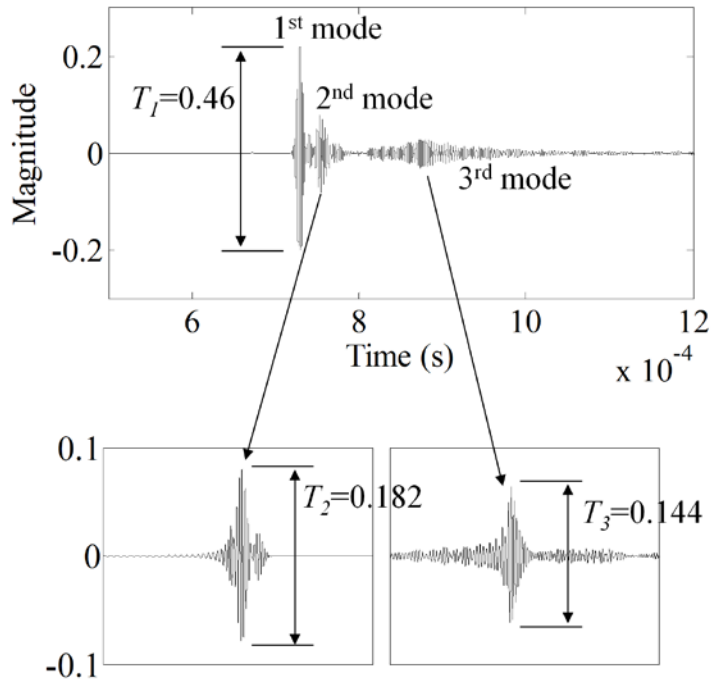

Figure 6. 11. The measured signal for the notch defect notch which has 9-mm depth, 6-mm length and 200° central angle. Two dispersive modes; the second and third modes, should be compensated its dispersion.

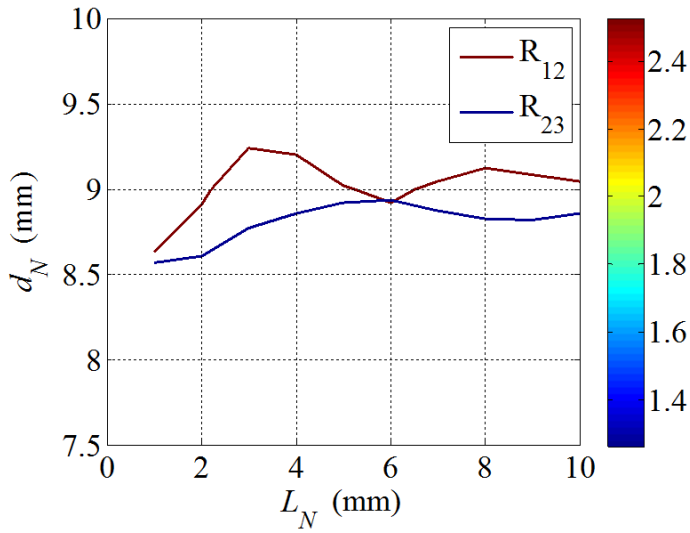

Figure 6. 12. Contour plots of ratios of R_{12} and R_{23} which are experimental results for a notch defect having 9-mm depth, 6-mm length and 200° central angle.

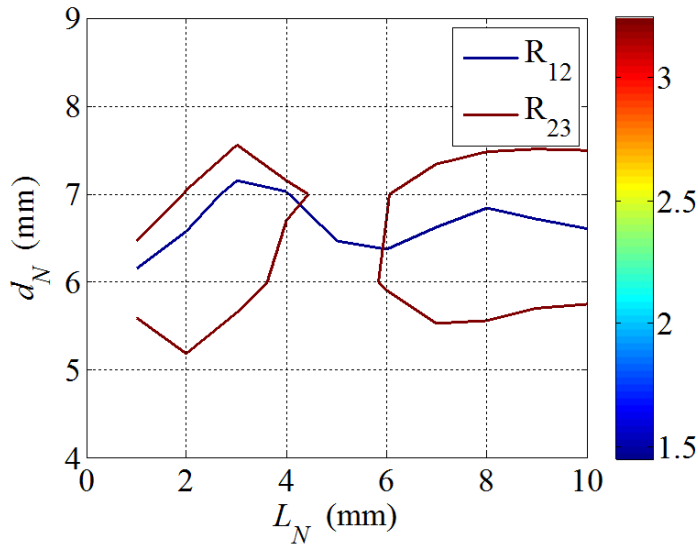

Figure 6. 13. Contour plots of ratios of R_{12} and R_{23} which are experimental results for a notch defect having 6-mm depth, 6-mm length and 200° central angle.

CHAPTER 7.

Conclusions

Quantitative characterization method of a part-circumferential notch defect which is defined as depth, length and central angle is developed. Three reflected torsional wave modes, from the first to third, are measured with respect to the incident first torsional wave mode. Ratios between three torsional modes are used to directly characterize depth and length of notch defect and then central angle can be predicted using linearity between the reflection coefficients and central angle of notch defect. As a reference, axisymmetric notch scattering theory is investigated. Schematic explanatory for whole procedure of the proposed notch characterization method as followings;

1) Need in advance

- Geometry of test pipe (Radius and thickness)
- Properties of test pipe (including dispersion relation)

2) Experiments

- Excite only the first torsional wave mode at a frequency above second cut-off frequency
- Measure the first, second and third torsional wave modes

3) Signal processing

- Dispersion compensation method to obtain reflection coefficients of dispersive modes (the second and third modes)

4) Estimation of depth and length

- Two ratios between three reflection coefficients
- Constructive contours of ratios from reference having the values obtained through experiment
- Intersections can be candidates
- Additional consideration of signal shapes for non-unique cases

5) Estimation of central angle

- Comparison reflection coefficients to references (under axisymmetric assumption) using linearity between the reflection coefficients and central angle of notch defect.

Unfortunately, the proposed method occasionally predicts a couple of candidates. Because signal comparing to overcome this needs particular efforts and precise experiments, selection of proper values among candidates is sometimes unavailable. In this case, if one applies existing method to characterize notch length (using several waves with difference frequencies), depth and central angle can be uniquely predicted.

Through practical experiments for the artificial notch defects, the effectiveness of the proposed method has been demonstrated.

REFERENCES

[1] M. J. Lowe, D. N. Alleyne, and P. Cawley, "Defect detection in pipes using guided waves," *Ultrasonics,* vol. 36, pp. 147-154, 1998.

[2] D. Guo and T. Kundu, "A new transducer holder mechanism for pipe inspection," *The Journal of the Acoustical Society of America,* vol. 110, pp. 303-309, 2001.

[3] J. Barshinger, J. L. Rose, and M. J. Avioli, "Guided wave resonance tuning for pipe inspection," in *ASME 2002 Pressure Vessels and Piping Conference*, 2002, pp. 49-62.

[4] W.-B. Na and T. Kundu, "Underwater pipeline inspection using guided waves," *Journal of pressure vessel technology,* vol. 124, pp. 196-200, 2002.

[5] W.-B. Na and T. Kundu, "EMAT-based inspection of concrete-filled steel pipes for internal voids and inclusions," *Journal of pressure vessel technology,* vol. 124, pp. 265-272, 2002.

[6] J. L. Rose, "Ultrasonic guided waves in structural health monitoring," *Key Engineering Materials,* vol. 270, pp. 14-21, 2004.

[7] J. L. Rose, M. J. Avioli, P. Mudge, and R. Sanderson, "Guided wave inspection potential of defects in rail," *Ndt & E International,* vol. 37, pp. 153-161, 2004.

[8] J. Ma, F. Simonetti, and M. Lowe, "Scattering of the fundamental torsional mode by an axisymmetric layer inside a pipe," *The Journal of the Acoustical Society of America,* vol. 120, pp. 1871-1880, 2006.

[9] W. Luo and J. L. Rose, "Phased array focusing with guided waves in a viscoelastic coated hollow cylinder," *The Journal of the Acoustical Society*

of America, vol. 121, pp. 1945-1955, 2007.

[10] W. Grandia and C. Fortunko, "NDE applications of air-coupled ultrasonic transducers," *Proc. IEEE Ultrasonics symp.,* vol. 1, pp. 697-709, 1995.

[11] D. N. Alleyne and P. Cawley, "The excitation of Lamb waves in pipes using dry-coupled piezoelectric transducers," *J. Nondestruct. Eval.,* vol. 15, pp. 11-20, Mar. 1996.

[12] J. L. Rose, "Guided wave nuances for ultrasonic nondestructive evaluation," *IEEE Trans. Ultrason. Ferroelectr. Freq. Control,* vol. 47, pp. 575-583, May 2000.

[13] H. Kwun, S. Y. Kim, and J. F. Crane, "Method and apparatus generating and detecting torsional wave inspection of pipes or tubes," U.S. patent Patent US 6,429,650 B1, 2002.

[14] A. Demma, P. Cawley, M. Lowe, A. Roosenbrand, and B. Pavlakovic, "The reflection of guided waves from notches in pipes: a guide for interpreting corrosion measurements," *Ndt & E International,* vol. 37, pp. 167-180, 2004.

[15] Y. Y. Kim, C. I. Park, S. H. Cho, and S. W. Han, "Torsional wave experiments with a new magnetostrictive transducer configuration," *J. Acoust. Soc. Am.,* vol. 117, pp. 3459-3468, Jun. 2005.

[16] A. Panda, P. K. Sharan, R. Roy, G. Murthy, and A. Mitra, "Generation and detection of guided waves in a defective pipe using rapidly quenched magnetostrictive ribbons," *Smart Materials and Structures,* vol. 21, p. 045015 (8pp), 2012.

[17] M. Saka and M. S. Akanda, "Ultrasonic measurement of the crack depth

and the crack opening stress intensity factor under a no load condition," *J. Nondestr. Eval.,* vol. 23, pp. 49-63, 2004.

[18] J. Ma, M. Lowe, and F. Simonetti, "Feasibility study of sludge and blockage detection inside pipes using guided torsional waves," *Meas. Sci. Tech.,* vol. 18, pp. 2629-2641, Jul. 2007.

[19] J. Mu, L. Zhang, and J. Rose, "Defect circumferential sizing by using long range ultrasonic guided wave focusing techniques in pipe," *Nondestructive Testing and Evaluation,* vol. 22, pp. 239-253, 2007.

[20] S. Wooh and Y. Shi, "Synthetic phase tuning of guided waves," *IEEE Trans. Ultrason. Ferroelectr. Freq. Control,* vol. 48, pp. 209-223, Jan. 2001.

[21] T. Hayashi and M. Murase, "Defect imaging with guided waves in a pipe," *J. Acoust. Soc. Am.,* vol. 117, pp. 2134-2140, 2005.

[22] H. W. Kim, J. K. Lee, and Y. Y. Kim, "Circumferential phased array of shear-horizontal wave magnetostrictive patch transducers for pipe inspection," *Ultrasonics,* vol. 53, pp. 423-431, 2012.

[23] D. Alleyne, M. Lowe, and P. Cawley, "The reflection of guided waves from circumferential notches in pipes," *Journal of Applied mechanics,* vol. 65, pp. 635-641, 1998.

[24] M. Lowe, D. Alleyne, and P. Cawley, "The mode conversion of a guided wave by a part-circumferential notch in a pipe," *Journal of Applied mechanics,* vol. 65, pp. 649-656, 1998.

[25] A. Demma, P. Cawley, M. Lowe, and A. G. Roosenbrand, "The reflection of the fundamental torsional mode from cracks and notches in pipes," *J. Acoust. Soc. Am.,* vol. 114, pp. 611-625, Aug. 2003.

[26] X. Wang, P. W. Tse, C. K. Mechefske, and M. Hua, "Experimental investigation of reflection in guided wave-based inspection for the characterization of pipeline defects," *Ndt & E International,* vol. 43, pp. 365-374, 2010.

[27] W. Zhou, M. Ichchou, and J. Mencik, "Analysis of wave propagation in cylindrical pipes with local inhomogeneities," *Journal of Sound and Vibration,* vol. 319, pp. 335-354, 2009.

[28] M. Silk and K. Bainton, "The propagation in metal tubing of ultrasonic wave modes equivalent to Lamb waves," *Ultrasonics,* vol. 17, pp. 11-19, 1979.

[29] D. C. Gazis, "Three-Dimensional Investigation of the Propagation of Waves in Hollow Circular Cylinders. I. Analytical Foundation," *J. Acoust. Soc. Am.,* vol. 31, pp. 568-573, May 1959.

[30] J. Rose, "Ultrasonic waves in solid media," ed: Cambridge University Press, 1999.

[31] P. D. Wilcox, "A rapid signal processing technique to remove the effect of dispersion from guided wave signals," *Ultrasonics, Ferroelectrics and Frequency Control, IEEE Transactions on,* vol. 50, pp. 419-427, 2003.

[32] H. E. Engan, "Torsional wave scattering from a diameter step in a rod," *The Journal of the Acoustical Society of America,* vol. 104, pp. 2015-2024, 1998.

[33] K. F. Graff, *Wave motion in elastic solids*: Dover Pubns, 1975, pp. 464-480.

[34] I. S. Gradshteyn, I. M. Ryzhik, A. Jeffrey, D. Zwillinger, and S. Technica, *Table of integrals, series, and products* vol. 6: Academic press New York,

1965.

[35] Y. L. Luke, *Integrals of Bessel functions*: McGraw-Hill New York, 1962.

[36] B. Pavlakovic, M. Lowe, D. Alleyne, and P. Cawley, "Disperse: a general purpose program for creating dispersion curves," in *Review of progress in quantitative nondestructive evaluation,* ed: Springer, 1997, pp. 185-192.

[37] COMSOL, "Comsol Multiphysics Modeling Guide: Version 3.5COMSOL AB, Stockholm, 2008."

[38] W. Zhuang, S. Datta, and A. Shah, "Axisymmetric guided wave scattering by cracks in welded steel pipes," *Journal of pressure vessel technology,* vol. 119, pp. 401-406, 1997.

[39] H. Bai, A. Shah, N. Popplewell, and S. Datta, "Scattering of guided waves by circumferential cracks in steel pipes," in *REVIEW OF PROGRESS IN QUANTITATIVE NONDESTRUCTIVE EVALUATION: Volume 20,* 2001, pp. 188-195.

[40] J. M. Galán and R. Abascal, "Numerical simulation of Lamb wave scattering in semi-infinite plates," *International Journal for Numerical Methods in Engineering,* vol. 53, pp. 1145-1173, 2002.

[41] X. Zhao and J. L. Rose, "Boundary element modeling for defect characterization potential in a wave guide," *International Journal of Solids and Structures,* vol. 40, pp. 2645-2658, 2003.

[42] D. Mead, "A general theory of harmonic wave propagation in linear periodic systems with multiple coupling," *Journal of Sound and Vibration,* vol. 27, pp. 235-260, 1973.

[43] A. Bocquillet, M. Ichchou, and L. Jezequel, "Energetics of axisymmetric

fluid-filled pipes up to high frequencies," *Journal of fluids and structures*, vol. 17, pp. 491-510, 2003.

[44] L. Houillon, M. Ichchou, and L. Jezequel, "Wave motion in thin-walled structures," *Journal of Sound and Vibration*, vol. 281, pp. 483-507, 2005.

[45] B. R. Mace, D. Duhamel, M. J. Brennan, and L. Hinke, "Finite element prediction of wave motion in structural waveguides," *The Journal of the Acoustical Society of America*, vol. 117, pp. 2835-2843, 2005.

[46] D. Duhamel, B. R. Mace, and M. J. Brennan, "Finite element analysis of the vibrations of waveguides and periodic structures," *Journal of Sound and Vibration*, vol. 294, pp. 205-220, 2006.

[47] M. Ichchou, S. Akrout, and J.-M. Mencik, "Guided waves group and energy velocities via finite elements," *Journal of Sound and Vibration*, vol. 305, pp. 931-944, 2007.

[48] J.-M. Mencik and M. Ichchou, "Wave finite elements in guided elastodynamics with internal fluid," *International Journal of Solids and Structures*, vol. 44, pp. 2148-2167, 2007.

[49] Dassault, "Abaqus 6.10: Analysis user's manual," *Providence, RI: Dassault Systèmes Simulia Corp*, 2010.

[50] H. W. Kim, Y. E. Kwon, J. K. Lee, and Y. Y. Kim, "Higher torsional mode suppression in a pipe for enhancing the first torsional mode by using magnetostrictive patch transducers," *IEEE transactions on ultrasonics, ferroelectrics, and frequency control*, vol. 60, pp. 562-572, Mar. 2013.

[51] R. B. Thompson, "Generation of horizontally polarized shear waves in ferromagnetic materials using magnetostrictively coupled meander coil

electromagnetic transducers," *Appl. Phys. Lett.*, vol. 34, pp. 175-177, 1979.

[52] D. Jiles, "Theory of the magnetomechanical effect," *J. phys. D: Appl. Phys.*, vol. 28, pp. 1537-1546, 1995.

[53] J. Rose, S. Pelts, and M. Quarry, "A comb transducer model for guided wave NDE," *Ultrasonics*, vol. 36, pp. 163-169, Feb. 1998.

[54] J. S. Lee, Y. Y. Kim, and S. H. Cho, "Beam-focused shear-horizontal wave generation in a plate by a circular magnetostrictive patch transducer employing a planar solenoid array," *Smart Mater. Struct.*, vol. 18, p. 015009, 2009.

[55] S. H. Cho, H. W. Kim, and Y. Y. Kim, "Megahertz-range guided pure torsional wave transduction and experiments using a magnetostrictive transducer," *IEEE Trans. Ultrason. Ferroelectr.*, vol. 57, pp. 1225-1229, 2010.

[56] H. W. Kim, Y. E. Kwon, S. H. Cho, and Y. Y. Kim, "Shear-horizontal wave-based pipe damage inspection by arrays of segmented magnetostrictive patches," *IEEE Trans. Ultrason. Ferroelectr.*, vol. 58, pp. 2689-2698, 2011.

ABSTRACT (KOREAN)

비틀림파의 산란 이론과 복수의 비틀림 모드를 활용한 노치 결함의 정량화 기법

Torsional wave scattering theory in a pipe and notch defect characterization using multiple torsional wave modes

권 영 의
서울대학교 대학원
기계항공공학부

본 연구는 배관에서 부분 노치 결함을 정량적으로 평가하기 위한 기법의 개발을 다루었다. 지금까지 노치 결함의 크기를 평가하기 위한 연구들이 수행되어 왔지만, 결함의 모든 정보를 정량적으로 평가 할 수 있는 방법은 보고되지 않았다. 부분 노치 결함의 크기를 진단 할 수 있는 획기적으로 향상된 방법을 고안하기 위해서, 3차 모드까지 존재하는 주파수 영역에서 비틀림파의 1차 모드만을 선별적으로 가진하고 결함으로부터 반사되는 1, 2, 3차 비틀림 모드를 측정하는 방법을 제안하였다. 기존에

굽힘파를 이용하는 연구들은 있었으나, 고차의 비틀림 모드를 사용하는 방법은 존재하지 않았다. 복수의 비틀림 모드를 사용하는 경우에는 모든 비틀림 모드가 축 대칭이기 때문에 반사 계수의 크기가 노치 결함의 중심각에 비례하여 증가한다는 장점이 있다. 그러므로 비틀림 모드들의 반사 계수의 비(比)를 고려하면 이 값이 노치 결함의 중심각과는 무관한 결과를 나타내어 결함의 깊이와 길이를 직접적으로 정량화하는데 이용할 수 있다.

결함의 크기를 정량화 하기 위해서는 결함에 대한 기준 정보 (reference)가 필요하다. 기존에 굽힘파를 사용하는 연구들은 삼차원 해석 결과를 기준으로 필요로 했지만, 본 연구에서는 축대칭인 비틀림파만을 사용하기 때문에 축 대칭 노치 결함에 대한 기준 정보만 필요로 한다. 이를 위해 본 연구에서는 새롭게 축대칭 부분 노치의 산란 이론을 제시하였다. 이를 이용하여 반사 계수들의 비에 해당하는 등-반사계수 윤곽선(equi-reflection coefficient contour)을 그리면 결함의 깊이와 길이를 예측할 수 있다. 비틀림파의 고차 모드는 분산 특성을 갖기 때문에 고차 모드들의 반사 계수를 구하기 위해서는 분산 보상 방법(dispersion compensation method)을 적용하여야 한다. 이 방법을 통해 결함에서 반사되는 순간 각 모드의 크기와 형태가 어떻게 나타나는지 계산할 수 있다. 개발된 축대칭 노치 분산 이론은 실험적으로 검증되었다. 실제 노치 결함의 정량화 실험을 통하여 제안된 방법의 효율성을 입증하였다.